Measurement of ^{236}U, ^{137}Cs, and ^{129}I in the Labrador and Beaufort Seas

Daniel Clifford Sauvé

Thesis submitted to the

Faculty of Graduate and Postdoctoral Studies in
partial fulfillment of the requirements for the

Specialization MSc degree in Environmental and Chemical Toxicology (Earth Sciences)

Ottawa-Carleton Geoscience Centre

Department of Earth Sciences

Faculty of Science

University of Ottawa

January, 2016

Abstract

The first comprehensive analysis of surface waters in the Labrador Sea for ^{236}U was completed via Accelerator Mass Spectrometry. Through the analysis of ^{236}U the method for AMS measurement was fine-tuned to allow for more precise results. Surface samples for the anthropogenic isotopes ^{137}Cs and ^{129}I were also collected along with two depth profiles of ^{129}I.

Samples were also collected in the Beaufort Sea and analyzed for the aforementioned isotopes. It was found that anthropogenic ^{129}I from reprocessing plants is easily discernible at different concentrations among water bodies in both the Labrador and Beaufort Sea. ^{137}Cs in surface waters is close to global fallout levels with no discernable influence from reprocessing plant inputs, but follows a similar trend to that of ^{129}I with depth in the Beaufort Sea. ^{236}U among surface waters in the Labrador Sea did not follow the same trends as ^{129}I but had concentrations indicative of a mix of global fallout as well as reprocessing plant influenced waters. ^{236}U samples from the Beaufort Sea were contaminated by an unknown source of ^{236}U and were inconclusive but were reproducible and allowed for continued development of the AMS analysis methodology.

Resumé

La première analyse complète des eaux de surface dans la mer du Labrador pour ^{236}U a été recueillie par spectrométrie de masse par accélérateur (SMA). Grâce à l'analyse de ^{236}U, la méthodologie analytique par SMA a était raffinée pour permettre des résultats plus précis. Les échantillons supplémentaires ont été recueillis pour mesurer les isotopes anthropique ^{137}Cs et ^{129}I ainsi que deux profiles supplémentaires pour ^{129}I.

Plusieurs autres échantillons ont aussi été récoltés dans la mer Beaufort pour les isotopes anthropiques susmentionnés. Il fut observé que l'isotope anthropique ^{129}I qui dérive des usines de traitement des combustibles nucléaires usés, est facilement perceptible par les différentes concentrations des plans d'eau des mers de Labrador et Beaufort. ^{137}Cs, dans les eaux de surface, est proche des valeurs pour les retombées radioactives globale sans une influence perceptibles des usines de traitement des combustibles nucléaires usés. Cependant, il suit une tendance similaire en profondeur à la valeur de l'isotope ^{129}I dans la mer Beaufort. Dans la mer Labrador, ^{236}U ne suit pas les tendances de ^{129}I mais reflète plutôt des concentrations indicatives d'un mélange de retombe radioactive et d'eau ternie par les usines de traitement des combustibles nucléaires usés. Les échantillons de ^{236}U recueillies dans la mer de Beaufort ont été pollués par une source inconnue de ^{236}U desquels aucune conclusion ne pouvait être tirée mais qui sont reproductibles et qui ont permis l'élaboration continue dans la méthodologie analytique par SMA.

Acknowledgements

I would like to thank my supervisor for his continued support throughout the entirety of this project. His willingness to assist and lend his knowledge and expertise at all times was a major contributor to my success. I would also like to express my sincere thanks to the members of the A. E. Lalonde AMS lab, particularly Dr. Xiaolei Zhao and Cole MacDonald for their assistance in the technical side of my project. Furthermore, I would like to thank Dr. John Smith of the Bedford Institute of Oceanography for his support in the oceanographic aspects of my project as well as lending his knowledge and experience to aid in my field work. I would also like to thank the staff of the Canadian Coast Guard for their continued assistance and professionalism in the operation of the ice breakers I was aboard and their assistance in the sample collecting procedure. Finally, I would like to thank my friends and family whose unwavering support throughout the entirety of this project helped provide motivation for its completion.

Table of Contents

List of Figures

List of Tables

1. Introduction

The Arctic

In recent years, the Arctic has become a topic of increasing popularity in both political and environmental circles for varying reasons. The Arctic is usually defined as the region located above the Arctic Circle, located at latitude 66° 33' 46.1" N. This latitude marks the point where the sun does not set on the summer solstice, nor rise during the winter solstice (National Snow and Ice Data Center, 2015). However, there are two other common definitions of what makes up the Arctic. The first is what is called the Arctic tree line which denotes the point where trees cease to grow and the land becomes dominated by small shrubs as well as lichens (National Snow and Ice Data Center, 2015). Finally, the Arctic can be defined in terms of temperature, the boundary located where the average daily temperature for the warmest month does not rise above 10°C (National Snow and Ice Data Center, 2015). A map with the extent of each of these definitions can be found in Figure 1.

Figure 1: Extent on the Arctic based on the parameters of the Arctic Circle (broken blue circle), Arctic treeline (green line), and maximum temperature (red line). (National Snow and Ice Data Center, 2015)

With increasing temperatures caused by global climate change, the Arctic is

considered one of the most susceptible regions to these effects (Anisimov et al., 2008) with temperatures increasing in the Arctic at approximately twice the global rate (Anisimov et al., 2008; McBean et al., 2005). One of the significant effects of this warming trend has been the continued disappearance of sea ice. Sea ice refers to any type of ice that forms in or on the surface of the sea, formed by freezing sea water (Weeks, 2010). Since sea ice cover was first recorded in the 1970's the total area of sea ice has been shrinking with sea ice cover hitting record low levels (Comiso et al., 2015) with the lowest extent being recorded in 2015 (Figure 2). Sea ice loss has several implications, firstly in the loss of habitat to species native to the Arctic including the polar bears, which rely on sea ice for hunting (Laidre et al., 2015; Laidre et al., 2008) This, in turn, results in decreased biodiversity, as well as disruptions to the Arctic ecosystem (Laidre et al., 2015; Laidre et al., 2008). Furthermore sea ice loss has rendered the Arctic more hospitable for travel, opening up potential routes for shipping and trade, once impassible due to sea ice cover (Fuglestvedt et al., 2014; Lasserre, 2014). Trade

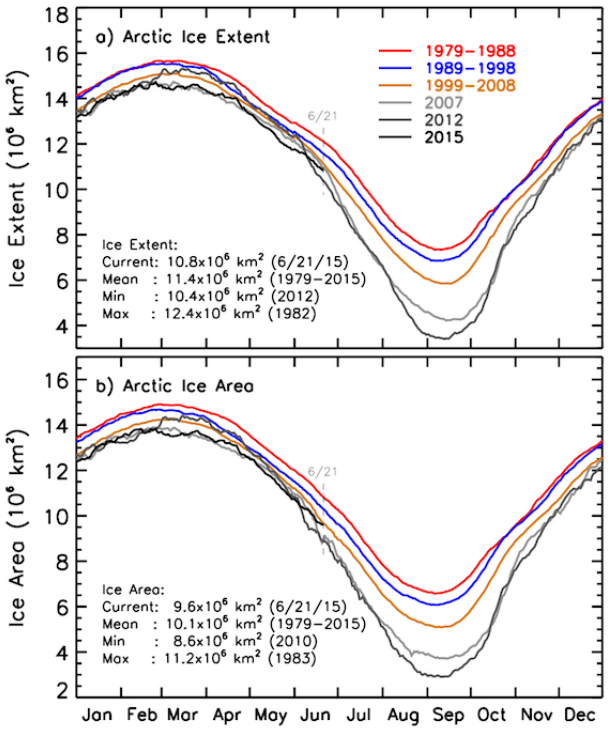

Figure 2: Annual sea ice extent from 1979 to present (Comiso et al., 2015)

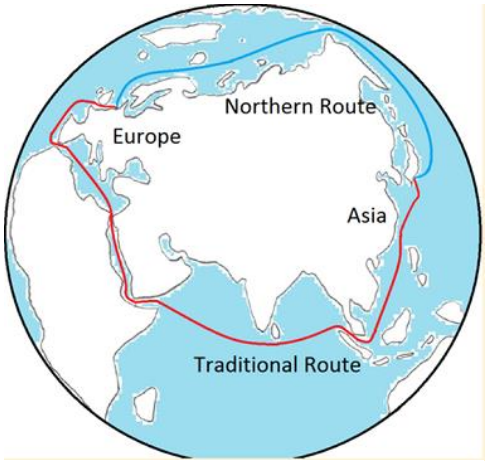

Figure 3: Potential Arctic shipping route (blue) compared to traditional route (red) Fuglesvedt et al., 2014

through the Arctic would provide a much shorter route from the Atlantic to the Pacific and Asia (Figure 3) and would therefore be more cost effective. Finally, nations bordering the Arctic have been in competition to decide territorial boundaries of this region as there is evidence of large deposits of fossil fuel, which are now accessible as well as cost effective due to the increasing hospitability of the Arctic (Osadetz et al., 2005).

Importance of Circulation in the Arctic

The Arctic plays an important role in global thermohaline circulation, and therefore the global climate. The primary role of the Arctic is to act as a balance in heat gain at low latitudes, and heat loss at high altitudes. (International Arctic Science Committee (IASC), 2010). Half of the excess heat produced at low latitudes is sent northwards as warm and salty water currents, while the other half travels towards the poles as atmospheric water vapour (IASC, 2010). Eventually, both these sources of heat reach the Arctic through ocean circulation as well as atmospheric transport. Heat carried in the atmosphere is released into the Arctic via condensation, adding fresh water to the Arctic system through precipitation. To avoid increased salinity at low latitudes, freshwater is imported from high latitudes such as the Arctic, returning to lower latitudes and reuniting atmospheric water with saline ocean water (IASC, 2010).

The Arctic also plays an important role in the global climate due to several feedback systems. First and most simply is the effect of sea ice on solar radiation and albedo. Ice and snow reflect solar radiation back into space more effectively than open water. With the warming of the Arctic, and less sea ice cover, more solar radiation is able to hit the oceans and warm the water, causing more sea ice melt, which again allows more solar radiation to be absorbed by the Arctic Ocean. Second is Thermohaline feedback. With increasing melting of Sea Ice, there is increased injection of fresh water into the Arctic Ocean. Increased export of fresh water from

the Arctic Ocean could lead to increased stratification in the North Atlantic Ocean, slowing down the global thermohaline current (THC). A slowed THC would draw less warm salty water from the low latitudes into the Arctic, slowing down global overturning and potentially leading to localized cooling due to less transport of heat via the oceans (IASC, 2010). Due to the highly important nature of the Arctic in the THC it is important to understand how currents and circulation in the Arctic function and to understand any potential changes that are occurring in the present day due to factors such as climate change.

1.3 Measuring Currents and Water Masses

Since the advent of nuclear technology, including nuclear weapons and nuclear power plants, the planet has been subject to large inputs of anthropogenically produced isotopes that in many cases have overwhelmed the natural inventories present on

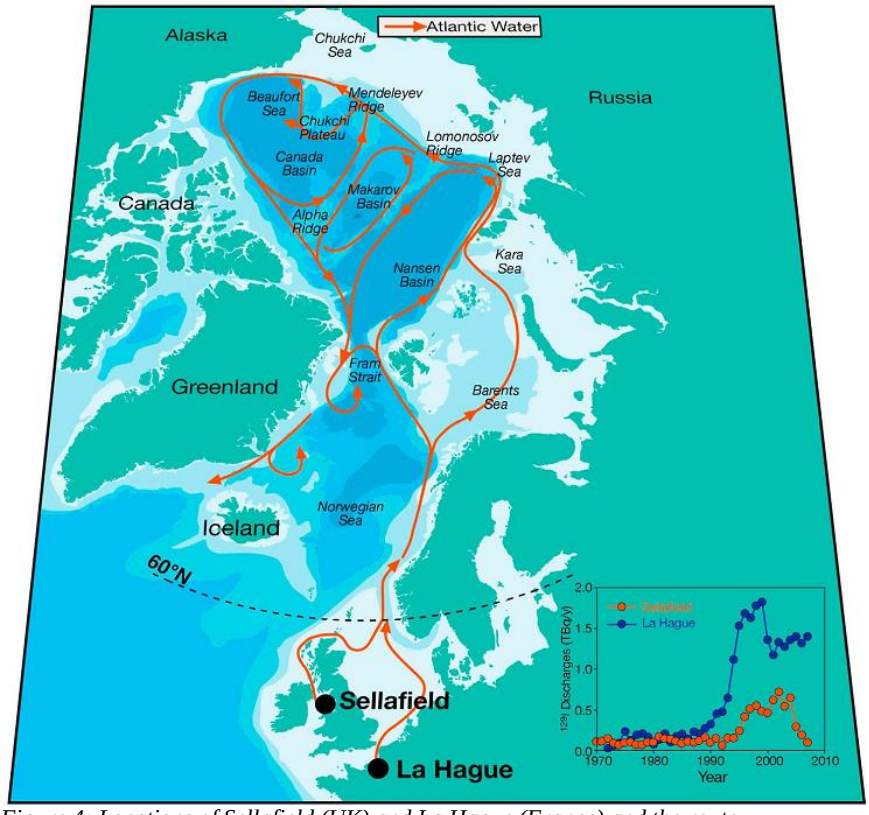

Figure 4: Locations of Sellafield (UK) and La Hague (France) and the route Radionuclide releases take into the Arctic Ocean. Inset: ^{129}I discharge data, Karcher et al., 2012

Earth (Casacuberta et al., 2014; Gómez-Guzmán et al., 2012; Christl et al., 2013) The presence of these isotopes in the environment provides a unique opportunity. Since the 1960's two nuclear reprocessing plants have been active in La Hague, France as well as Sellafield in the United Kingdom (Smith et al., 1998) (Figure 4). Through their operations they release radioisotopes into the environment at levels higher than the background in the surrounding water of the Irish Sea and English Channel (Smith and Ellis, 1999). This provides two large point source injections into the environment at concentrations significantly higher than background (Smith et al., 1998). The discharge information is relatively well documented since 1966 for La Hague and 1952 for Sellafield (Casacuberta et al., 2014) allowing the movement and timing of annual releases of radionuclides to be traced through Western European coastal waters. Three particular radioisotopes that have proven to be helpful in this task are characterized and documented below.

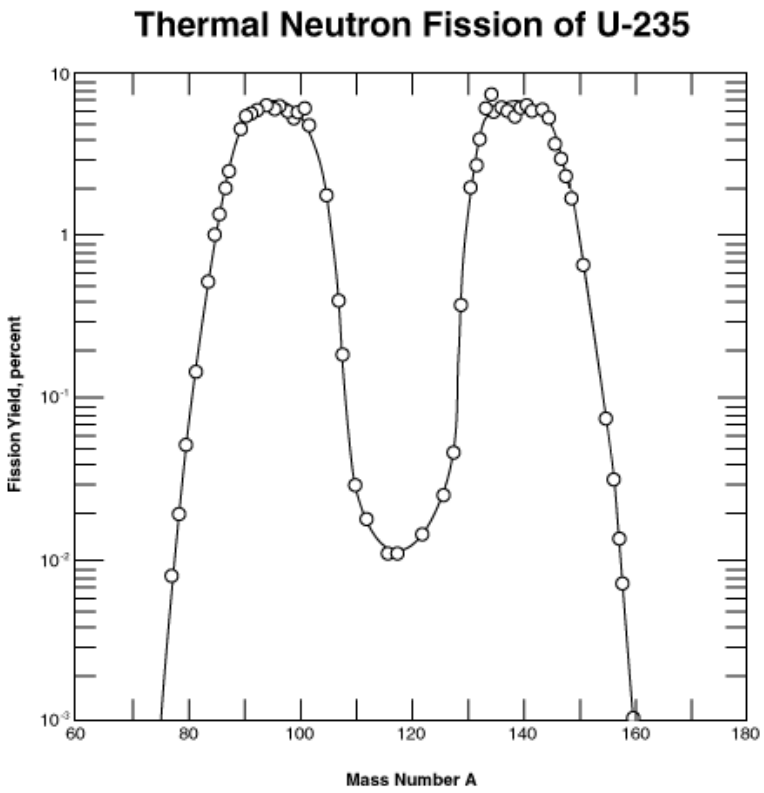

Figure 5: Fission Yield Curve of ^{235}U

Radioactive Isotopes as Tracers

^{129}I

Iodine-129 is a long lived radionuclide with a half-life of 15.7 Ma and has several natural sources. Firstly, it can be produced by bombardment of xenon in the atmosphere by cosmic rays. It is also a product of spontaneous fission of naturally occurring ^{238}U and ^{235}U in the lithosphere (Gómez-Guzmán et al., 2013) as well as rarely from neutron induced reactions on ^{128}Te and ^{130}Te. The natural production of ^{129}I has been found to produce $^{129}I/^{127}I$ ratios in a range of 10^{-12} to 10^{-13}. However as ^{129}I is a fission product of ^{238}U and ^{235}U with a yield of approximately 0.6% (Raisbeck et ela., 1995) it is also released into the environment from anthropogenic nuclear processes, including atmospheric nuclear weapons testing, incidents at Chernobyl and more recently Fukushima, as well as the activities of nuclear reprocessing plants (Gómez-Guzmán et al., 2013). These sources have increased the concentration of ^{129}I in the environment with anthropogenic ^{129}I changing the $^{129}I/^{127}I$ ratio to a range between 10^{-10} and 10^{-8} which corresponds to a concentration of between $1x10^8$ and $33.7x10^8$ atoms/L (Gómez-Guzmán et al., 2013).

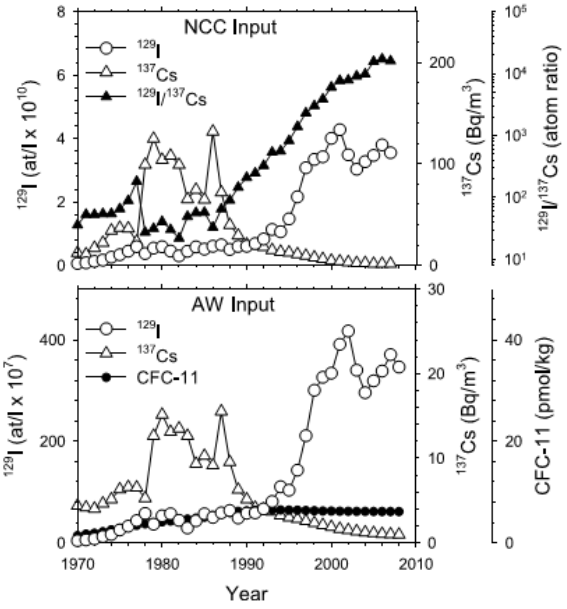

Figure 6: Inputs of ^{129}I and ^{137}Cs into the Norwegian Coastal Current at 60°N (top) and inputs for Arctic Water entering intermediate levels of the Arctic Ocean from the eastern Norwegian Sea (Smith et al., 2011)

Iodine, and by extension ^{129}I is biophilic and thus capable of entering the food chain (Gómez-Guzmán et al., 2013). Iodine is also capable of forming several compounds such as I_2, HI, HOI, CH_3I, and KI, which are both water soluble and volatile (Gómez-Guzmán et al., 2013) allowing for exchange across the air/water interface. These reactions are slow in the open ocean. ^{129}I will behave in a mostly conservative manner giving it an advantage over other tracers such as chlorofluorocarbons that rapidly exchange with the atmosphere (Raisbeck et al., 1995). As a by-product of the operation of nuclear reactors ^{129}I is one of the major isotopes released at the Sellafield and La Hague reprocessing locations, and as such provides two origins for its release into the environment. As is evident from Figure 6, the ^{129}I input into the Arctic and surrounding area has increased since the mid 1990's allowing for better detection as well as the ability to follow tracer plumes from year to year (Smith et al., 2011)

^{137}Cs

Cesium-137 with a half-life of 30.2 years (Smith et al., 1998) is formed as a fission product of ^{235}U at the very top of the fission/yield curve, meaning it has a fairly high rate of formation during the process of fission (Figure 5). Over time, it will build up in nuclear reactors and it is one of the isotopes removed during the reprocessing of spent nuclear fuel. Cesium-137 has been used as a tracer in ocean circulation since the 1970's, due to its ease of measurement through gamma spectroscopy. It is considered a useful radiotracer of ocean water due to its conservative behaviour in the open ocean, and therefore its distribution is largely controlled by advection and mixing of water (Cochran et al., 1995). Concentrations of ^{137}Cs have varied over the years due to input from global fallout of nuclear weapons testing debris, the nuclear reprocessing plants in Western Europe, as well as input in the late 1980's from the Chernobyl

incident. However, after the Chernobyl incident in 1986, visible in Figure 6, inputs of ^{137}Cs into the environment from reprocessing plants have decreased to negligible levels in recent years (Figure 6). Most of the ^{137}Cs presently entering the ocean from European sources (Figure 6) is due to runoff from the land or remobilization from marine sediments (Smith et al., 1998; 1999)

^{236}U

Uranium-236 is a long-lived and primarily anthropogenic isotope with a half-life of 23.4 Ma. It has several sources related to nuclear activities such as the testing of atomic weapons in the previous century and the release of nuclear waste, as well as releases from nuclear facilities such as nuclear power generating stations or nuclear reprocessing plants (Hotchkis et al., 2000). ^{236}U is produced when a ^{235}U atom is bombarded by a neutron. Approximately 80 per cent of the time this will result in the ^{235}U atom undergoing fission resulting in daughter atoms as well as the release of energy and neutrons to sustain the reaction. However, the remaining 20 per cent will stabilize into ^{236}U (Hotchkiss et al., 2000). Unfortunately, ^{236}U is non fissile and is therefore considered to have a "poisoning" effect on nuclear reactors where it will continue to capture neutrons without undergoing fission (Hotchkiss et al., 2000).

^{236}U can also be produced by neutron absorption of natural ^{235}U (Chamizo et al., 2015) However, it is estimated that only about 30kg of this naturally produced ^{236}U exists in the upper layers of the earth, with less than 0.5kg residing in the oceans (Eigl et al., 2012) with pre-anthropogenic $^{236}U/^{238}U$ ratios ranging from 10^{-14} to 10^{-10} (Steier et al., 2008). These values are outweighed by the anthropogenic inputs of ^{236}U into the environment, estimated to be approximately 10^{6}kg produced from nuclear reactors (Casacuberta et al., 2014) as well as about

900kg from atmospheric nuclear weapons tests (Christl et al., 2013). These ^{236}U inputs may be extremely useful as an oceanographic tracer since even a small amount of ^{236}U released into the oceans is enough to overwhelm the natural ^{236}U present (Casaberta et al., 2014) Furthermore it was observed by Sakaguchi et al., in 2011 that uranium, particularly ^{236}U, behaved conservatively. It remains dissolved in the water column and is not subject to scavenging after 50 years. This information implies that ^{236}U could be used as an effective long term oceanic tracer due to its behaviour and long half-life. One unfortunate shortcoming with respect to tracer applications of ^{236}U is that its discharge record from the aforementioned reprocessing plants has not been as extensively recorded as that for the other isotopes such as ^{137}Cs and ^{129}I (Casacuberta et al., 2014). Additional work is ongoing to address this issue.

Measuring low level isotopes

Among the aforementioned isotopes, Cesium-137 was the first to be widely used in oceanography in the 1960's (Smith et al., 1998) mainly due to its ease of measurement via Gamma spectrometry; although large volumes of water are required (20-100L). Iodine-129 and Uranium-236 however did not become available for measurement until much later, as the techniques and technology were simply not available. With the advent of Accelerator Mass Spectrometry (AMS) first ^{129}I and now more recently ^{236}U can be measured even at low concentrations in the Oceans. Furthermore, for the case of ^{129}I and ^{236}U, it is more efficient to use an atom counting method (as is used in AMS) than to use decay counting methods due to the low isotope concentrations and long half-lives of the isotopes in question (Kilius et al., 1992).

The main difference between regular mass spectrometry and AMS is the incorporation of a tandem accelerator into the analysis (beam) line. In the ion source a solid sample is sputtered with ^{133}Cs. The Cs ions collide with the atoms of the sample and release them from the sample

matrix. As these atoms leave the sample surface, the neutralized Cs which accumulates on the surface, gives up an electron to ionize them negatively. These ions are accelerated in a voltage gradient and injected into the beam line. The injection magnet performs a mass analysis and this ensures that atoms or molecules other than those with the masses of interest are unable to travel into the tandem accelerator. The tandem accelerator accelerates the molecules through a stripper, which is either in the form of a dense gas or thin carbon foil, which strips several electrons from the negative ions, forcing them into a positive state (Kilius et al., 1992; Zhao et al., 1997). Charge changing the ions into a positive state and selecting for a 3+ charge or higher ensures that only monoatomic ions pass through into the high energy beam line because the imbalance in the Coulomb forces resulting from changing the charge of the molecule disintegrate it into its constituent atoms. Finally, the positively charged ions pass through another magnet in which they are separated by mass, and then through an electrostatic analyzer that separates ions based on their energy to charge ratio. Then the ions are sent to detectors for measurement. Figure 7 below shows a visual summary of an AMS and its components.

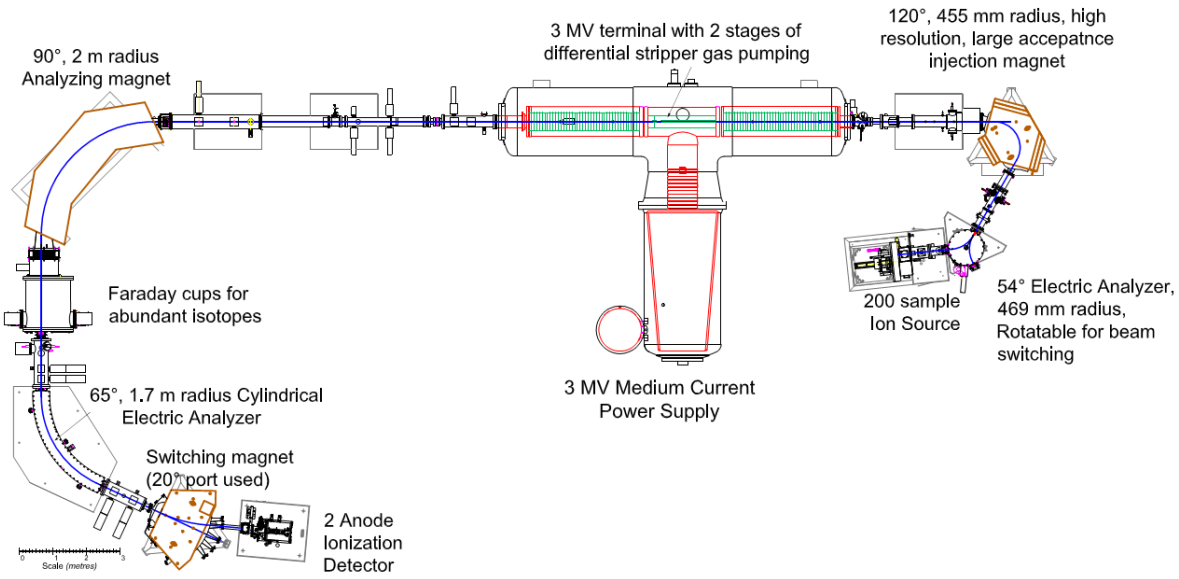

Figure 7: Diagram of the University of Ottawa AMS (Kieser et al., 2015)

Objectives

The objective of this thesis is to explore the utility of ^{236}U as a new potential tracer for water circulation in the Arctic alongside the anthropogenic isotopes ^{129}I and ^{137}Cs. It explores the development of a methodology for the analysis of ^{236}U from sea water via AMS and presents the first comprehensive analysis of ^{236}U in surface waters of the Labrador Sea as well as the first depth profile of ^{236}U in the Beaufort Sea. Using the ratio of $^{129}I/^{236}U$, conclusions will also be drawn on the origins of these anthropogenic tracers as well as the distribution of ^{236}U in the Labrador and Beaufort Sea when compared to the global distribution.

2. The Labrador Sea

The Labrador Sea is the body of water in the North Atlantic that divides the Labrador coast in Canada and the Greenland coast, the majority of which lies within the temperature zone defined as the Arctic (Figure 1) The Labrador Sea provides a unique opportunity for the measurement of radioisotopes, as there is a history of regular measurement. Since 1990, the Bedford Institute of Oceanography, a division of the Canadian Department of Fisheries and Oceans, has annually sampled a transect across the Labrador Sea (Yashayaev et al., 2014). This includes both chemical and biological measurements, along with more recent measurements for radionuclides such as ^{129}I (Smith et al., 2005).

2.1 Labrador Sea Water Masses

The Labrador Sea is important due to its location. As it borders the Arctic it is one of the few areas in which the Arctic Ocean interacts with the global ocean, in this case the North Atlantic. Like the Arctic Ocean, the Labrador Sea comprises several fairly distinct layers of water with their own characteristics. The upper Labrador Sea is dominated by the aptly named Labrador Sea water (LSW). During the winter, the flux of water and air associated with cold airflows over the Labrador Sea cause the formation of a convectively mixed surface layer, the depth of which depends on the severity of the winter (Lazier et al., 2002; Curry et al., 1998; Pickart et al., 2002). This provides the basis for the formation of Labrador Sea water, which in severe winters can reach depths greater than 2000 m (Lazier et al., 2002). The importance of Labrador Sea water is that the deep convection, which occurs in the Labrador Sea provides an important pathway for atmospheric gases such as oxygen, carbon dioxide, and Chlorfluoro-carbons to pass from the surface layers to intermediate depths (Lazier et al., 2002) signifying it

as one of the ocean's main "lungs" for the atmosphere-ocean exchange (Yashayaev et al., 2015). Due to the unique method of LSW formation, the convection present remixes and modifies it, changing its properties such as thickness, density, and salinity, so that many of its properties shift and change on an annual basis depending on seasonal conditions (Yashayaev et al., 2008). For simplicity, LSW can be considered to occupy the upper 2000 m of the central Labrador Sea (Yashayaev, 2007). Beneath the LSW layer lies the North East Atlantic Deep Water (NEADW), formed from the Iceland-Scotland overflow water (ISOW) (Yashayaev et al., 2015), which originates between Iceland and Scotland. This is formed primarily of older overflow waters, which are low in concentrations of anthropogenic tracers (Hansen and Osterhus, 2000). ISOW crosses the Mid-Atlantic ridge and flows northwards into the Irminger Sea, located between the Eastern Coast of Greenland and Iceland (Figure 8) and is carried into the Labrador Sea by the East Greenland Current (Smith et al., 2005). The NEADW layer separates the intermediate LSW layer from the bottom waters, which in the case of the Labrador Sea is composed of Denmark Strait Overflow Water (DSOW). DSOW is formed primarily of fresher returning Atlantic Water, which itself is partially formed from water travelling along the Norwegian Coastal Current following the Eastern Greenland Coast as part of the Eastern Greenland Current (Figure 8) as well as Arctic Intermediate Water. Upon entering the Irminger Sea, this DSOW descends off the Denmark Strait towards the bottom, where it is overridden by the ISOW water also travelling towards the Labrador Sea (Smith et al., 2005). Interestingly DSOW is actually less saline (34.84-34.87) than ISOW (34.92) but is kept in place by the halocline present between them as well as its increased density from low temperatures (Smith et al., 2005), which also allows for the two layers to be distinguished from one another. Therefore, the Labrador Sea can be characterized as three primary layers: the upper layer consisting of LSW in the first 2000 m,

underlain by a more saline NEADW layer which in turn overlies the DSOW found below 3000 m.

Figure 8: Overview of water masses and currents in and around the Labrador Sea, ISOW refers to Iceland-Scotland Overflow Water, DSOW refers to Denmark Strait Overflow Water, EGC is the Eastern Greenland Current, NAC the North Atlantic Current, NCC the Norwegian Coastal Current, RAW is Return Atlantic Water (Smith et al., 2005)

2.2 Labrador Sea Circulation

The Labrador Sea is one of the water bodies making up a major system in the greater Atlantic Ocean called Atlantic meridional overturning circulation (AMOC), which involves the northward flow of warm, salty water of the upper layers in the Atlantic, and the southward flow of colder waters from the north, deep Atlantic (Sundry, 2010). As mentioned above, the Labrador Sea plays an important part in the formation of LSW and in its role as one of the primary areas where overturn from increasing density occurs (Pickart and Spall, 2007).

The majority of water flows into the Labrador Sea from the east driven by several currents (Figure 8). On the Eastern side of Greenland, two currents flow side by side: the East Greenland current (EGC), which is primarily composed of cold, fresh water from the Arctic, while the Irminger Current (IC) is composed of warmer and saltier water. These two water masses flow around the Southern tip of Greenland and merge into the West Greenland Current (WGC). Some of this water flows up into Baffin Bay following the Greenland coast, however the majority of this current crosses the Labrador Sea before combining with water flowing out of the Davis Strait and flowing south along the North American coast and becoming the Labrador Current (Pickart and Spall, 2007). The Deep Western Boundary Current (DWBC) is located at the base of the continental slope and transports dense overflow water (such as the NEADW and DSOW discussed above) through the Labrador Sea and southward along the North American continental slope into the deep North Atlantic. Finally, the central Labrador Sea is primarily defined by a weak and nearly depth independent cyclonic gyre (Pickart and Spall, 2007; Lavender et al., 2000). A visual summary of the circulation of the Labrador Sea can be viewed in Figure 8 and Figure 9.

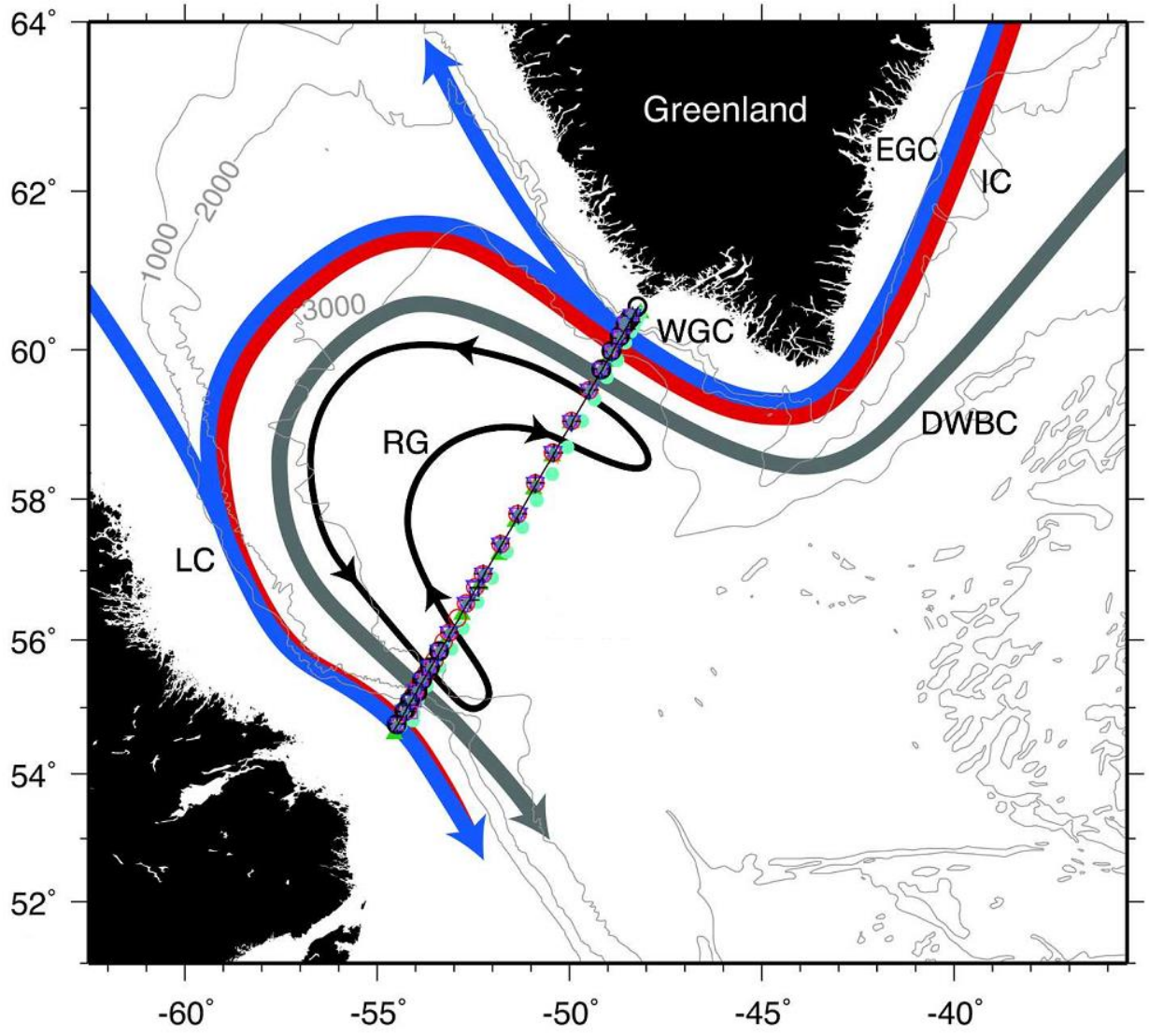

Figure 9: Dominant currents in the Labrador Sea. The Red line indicates warm upper layer current, while blue represents cold upper layer current. EGC refers to the East Greenland Current, IC is the Irminger Current, DWBC is the Deep Western Boundary Current, represented by the grey line, WGC is the West Greenland Current, LC is the Labrador Current, and RG as well as the black line refers to the recirculation gyre, (Pickart and Spall, 2007). Also pictured is the AR7W line and the stations occupied during this study

2.3 Labrador Sea Sampling Methods

^{129}I

Water was collected in two 1 litre bottles from each sampling site before being stored for analysis upon return to the University of Ottawa laboratory. For the analysis of ^{129}I no further preservation was required to store the samples. Surface samples were taken from along the AR7W line (Figure 10) in the Labrador Sea at every second station until reaching the Greenland Coast when samples were taken every station. Furthermore, two depth profiles for ^{129}I were taken at stations 17 and 24. The Iodine samples acquired can be reviewed in Table 1 along with the details of the depth profiles.

Table 1: Summary of Stations Sampled across the Labrador Sea line AR7W and their location; included in the two right columns are the details of the two depth profiles acquired.

Station ID	Depth	Latitude (N)	Longitude (W)	L3-17	L3-24
L3-05	4	54° 29.5′	54° 45.3′	510m	310m
L3-07	4	54° 57.3′	54° 17.7′	870m	560m
L3-09	4	55° 15.8′	53° 59′	1300m	880m
L3-11	4	55° 36.7′	53 37.9′	1550m	1060m
L3-13	4	56° 6.8′	53° 7′	2040m	1460m
L3-15	4	56° 57.4′	52° 14.2′	2520m	1860m
L3-17	4	57° 48′	51° 20.4′	2940m	2240m
L3-19	4	58° 38.4′	50° 25′	3120m	2400m
L3-21	4	59° 29′	49° 28.5′	3380m	2540m
L3-24	4	60° 10.5′	48° 40.5′	3490m	2760m
L3-25	4	60° 17.5′	48° 32.5′	3590m	2840m
L3-26	4	60° 22′	48° 27.2′	3670m	2900m
L3-27	4	60° 26.8′	48° 21.7′		
L3-28	4	60° 34′	48° 13.7′		

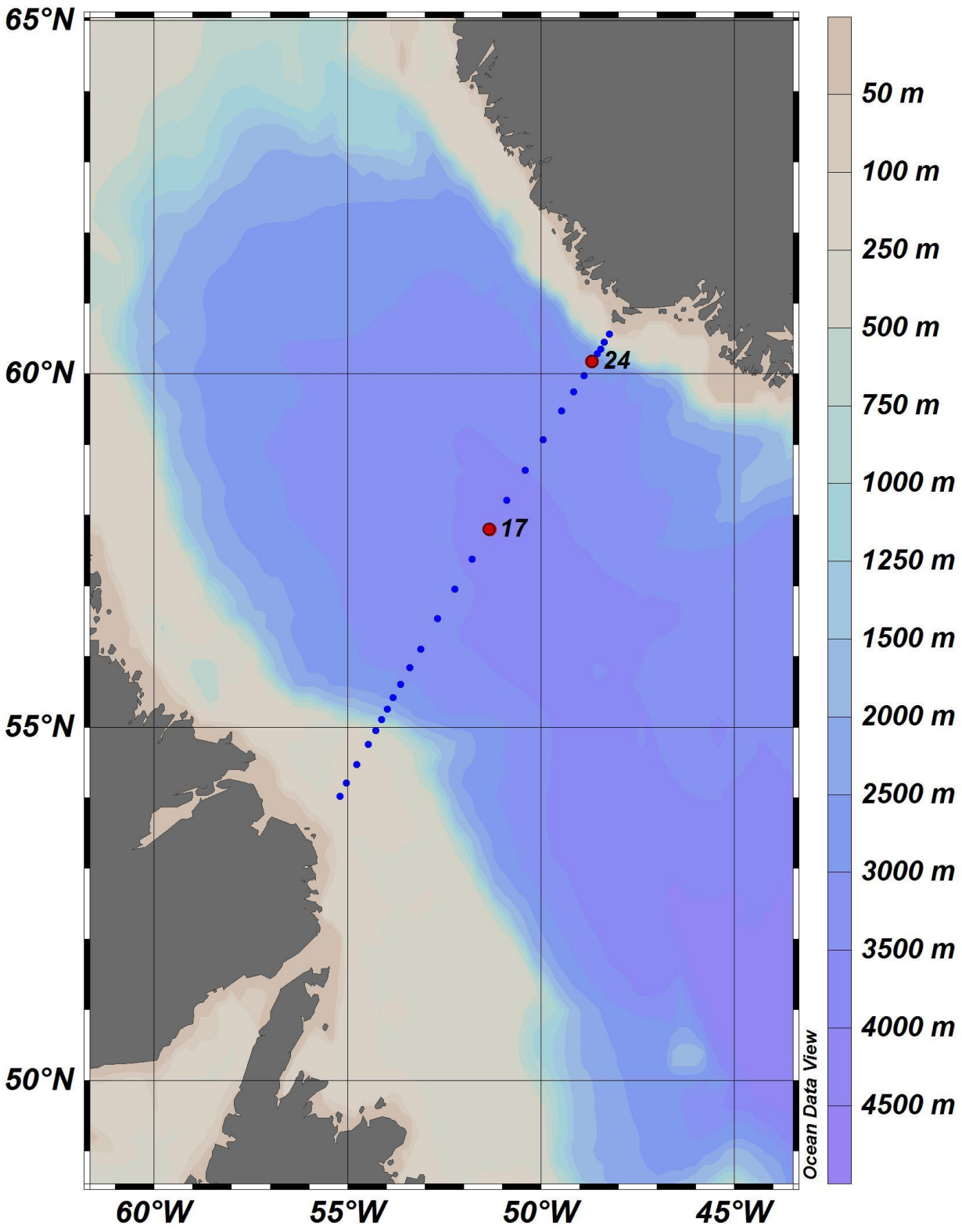

Figure 10: Labrador Sea Station Map, depth profile stations 17 and 24 are labelled

^{137}Cs

Seawater surface samples for cesium analyses were collected using the ships internal water intake system and stored in two hardware store buckets lined with plastic bags. The samples of 15 litres of seawater were weighed and 100 micrograms of ^{133}Cs was added in a 5 ml solution to act as a yield tracer. The water in the buckets was mixed and then a 20 ml subsample was removed for future analysis. The sample was then acidified to pH 2 using 20 ml of HNO_3. Four grams of Ammonium Phosphomolybdate (AMP) was added as a cesium sorbent, after the sample was acidified to facilitate sorption of cesium to the sorbent. The sample was then mixed and let stand for about 24 hours to allow for the precipitate to settle. The supernatant was removed and the sides of the bags were washed to remove the AMP precipitate. The sample was then transferred to increasingly smaller containers until the volume was able to fit in 1-3 50 ml centrifuge tubes. This methodology was modified from Sakaguchi et al., 2012. Unfortunately, due to the speed of station turnover close to the Greenland Coast along with the slow settling time of the AMP, no Cesium samples were acquired from stations 25 or 28.

^{236}U

To acquire uranium samples two plastic hardware store buckets were lined with plastic bags and each filled with 15 litres of seawater; 5.22 picograms of ^{233}U was added as a yield tracer to the water, and a 20 ml subsample was taken for ICP-MS analysis of ^{238}U. The sample was then acidified to pH 1-2 by adding 20 ml of concentrated HNO_3 and mixed thoroughly to ensure proper mixing. 400 mg of iron was then added to the water as $FeCl_3$ to coprecipitate the uranium. The acidified sample was then bubbled with Nitrogen gas for 20 minutes to remove any carbonates from the water, which would have otherwise preferentially complexed the

uranium and prevented it from coprecipitating with the iron hydroxide. To precipitate the $Fe(OH)_3$, the pH of the sample was then raised to 8-9 using 25 ml of concentrated NH_3OH. The sample was then covered and left so that the precipitate could settle. Once the sample had settled the supernatant was siphoned off and the remaining water and precipitate was transferred to a 2 litre graduated cylinder and left to resettle, after which more supernatant was removed. The process was repeated until the volume was small enough for the precipitate to be stored in 2-3 50 ml centrifuge tubes. This methodology was modified from Sakaguchi et al., 2012 . Surface sample duplicates were acquired from each station mentioned in table 1. Unfortunately, no large volume samples were acquired from the depth profiles due to limitations on the water budget.

2.4 Sample Analysis

^{129}I

Iodine was extracted from sea water using the following procedure adapted from The Protocol for the Analysis of Iodine-129 at the IsoTrace Laboratory manual, which is based on Fehn et al., 1992. 100 ml of seawater sample was added to a Nalgene bottle, 20µL of a Sodium Iodide carrier containing 2 mg of I was then added to the sample, and a further 100 ml of seawater was then added to the bottle to ensure thorough mixing of the NaI carrier. Iodate in the samples was then reduced to Iodine by adding 2 ml of 1 M Sodium Bisulfite, and the samples were shaken vigorously for 15 minutes and then left to stand for 16 hours.

Following the standing period, 15 ml of hexane was added to the solution and the reduced Iodine was oxidized to I_2 using 0.3 ml of 6 M Sodium Nitrite. The samples were then shaken vigorously for 15 minutes to maximize the transfer of the elemental Iodine into the organic phase. The hexane was then collected from the sample and stored. The Iodine extraction was

repeated two more times using 15 ml of hexane and then with 10 ml of hexane to ensure the collection of the majority of the Iodine from the sample.

The 40 ml of collected hexane was then re-added to the separatory funnel along with 10 ml of water. The Iodine was then reduced to I^- using 0.2 ml of 1 M Sodium Bisulfate, transferring the Iodine back into the aqueous phase. The water was then collected and the hexane discarded. The water was acidified using 0.2 ml of concentrated nitric acid to achieve a pH of 1, 15 ml of hexane was then added to the water along with 0.2 ml of 6 M Sodium Nitrite to force the Iodine back into the organic phase; the hexane was then collected. The Iodine was again reduced into the aqueous phase as described above. This process of transferring the Iodine between the organic and aqueous phase was to ensure the sample was a clean as possible, removing potential contaminants left in the discarded phases of each step. 0.1 ml of concentrated nitric acid was then added to the 10 ml sample and was heated to 85-90°C to remove any sulphur dioxide from the sample. 0.1 ml of 0.1 M Silver Nitrate was then added to the sample to precipitate the Iodine as Silver Iodide. The precipitate was allowed to settle, then collected and dried.

The Iodine was then mixed with pure Niobium powder roughly in a 4:1 mixture of Niobium to Silver Iodide. The addition of Niobium is to facilitate conductivity in the sample as Silver Iodide is not very conductive. The samples were pressed into targets and run on the AMS at the University of Ottawa (Kieser et al. 2015).

^{137}Cs

Upon returning to the University of Ottawa the samples were centrifuged and remaining supernatant was removed, samples from the same station and depth were then consolidated into a single centrifuge tube and places into a drying oven for 24 hours to remove the remaining water. Afterwards the remaining AMP was weighed to measure physical recovery. 50 mg subsamples of AMP were removed and redissolved for use in ICP-MS to measure the ^{133}Cs added as a spike to record the chemical recovery of the ^{137}Cs by the AMP. Due to the low amount of ^{133}Cs added to the samples however it was necessary to look at other possible inputs of ^{133}Cs due to the possibility that the majority of ^{133}Cs observed in the samples was coming from other sources rather than the spike. AMP without any added ^{133}Cs and unprocessed sea water was also analyzed for ^{133}Cs and it was found that the cumulative ^{133}Cs input from these sources accounted for approximately 3% of the ^{133}Cs observed in the samples, which has been corrected for in the calculations.

The remaining AMP was transferred to a vial and prepared for Gamma counting to measure the activity of ^{137}Cs. The samples were analyzed on a high resolution HPGe detector (Ortec Instruments Inc). Due to the low concentration of ^{137}Cs in the oceans, the samples were counted for an average of 2 days each in order to attain enough counts.

^{236}U

Upon return to the lab samples were centrifuged and any remaining supernatant was discarded. The iron precipitate was then consolidated and dissolved using 5 ml of 8 M HNO_3 which was then diluted to 4 M with 5 ml of deionized water. The dissolved sample was then run through a 1.2 micron filter to ensure any remaining solids were removed from the sample. To remove the uranium from the sample, UTEVA resin columns were used. The extractant in UTEVA resin is diamyl, amylphosphonate (DAAP) and will form nitrato complexes with actinide elements (Horwitz et al., 1992). These complexes are formed from the nitrate in the sample. This means that actinide uptake onto the resin from the sample is driven by increasing concentration of nitric acid (Horwitz et al., 1992). Furthermore actinides can easily be stripped from the resin by use of very dilute nitric acid, however it was also noted that dilute hydrochloric acid was more efficient at removing actinides from the resin (Horwitz et al., 1992)

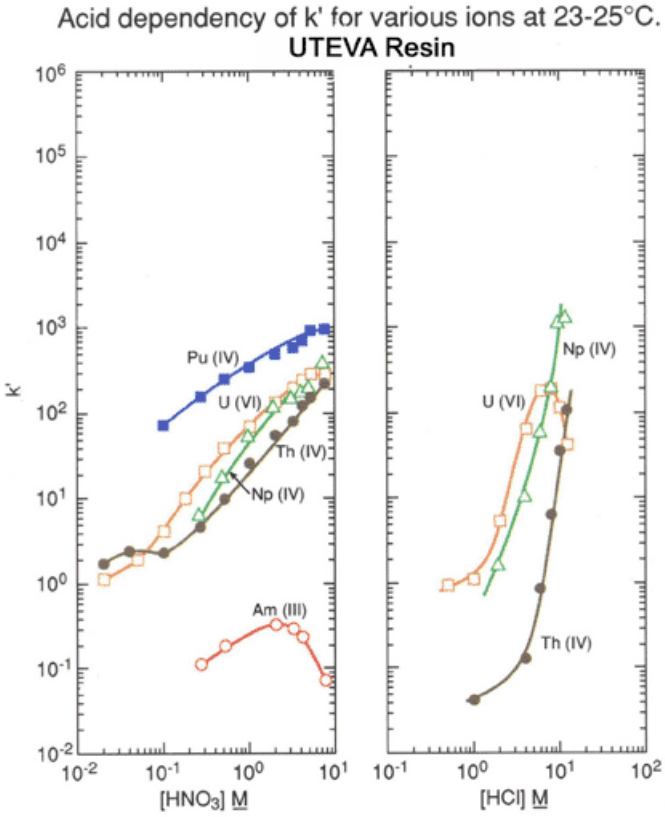

Figure 11: Horwitz et al., 1992 retrieved from: http://www.eichrom.com/products/info/uteva_resin.aspx

The UTEVA columns used were first equilibrated and activated by running 10 ml of 4 M HNO_3 through them, afterwards the sample was then mounted and allowed to run through the column. After the sample had been run through the column another 10ml of 4 M HNO_3 was

passed through the column to remove any additional iron that may have been left over, then 5 ml of 6 M HCl was passed through the column to remove any thorium that may have been present, after which only uranium was left on the column. The uranium was then eluted from the column into a clean centrifuge tube with 10 ml of 0.0025 M HCl. The sample was then placed in a drying bath for 24 hours to remove the HCl. After 24 hours, 4 mg of iron as a $FeCl_3$ solution was added to the vial as well as 5 ml of 0.5 M HNO_3. The sample was then shaken and concentrated ammonium hydroxide was added dropwise until the iron with the concentrated uranium reprecipitated. Again the sample was centrifuged and the supernatant was discarded leaving 4 mg of iron containing the concentrated uranium from the sea sample. The precipitate was then again dried for 24 hours before being transferred to a quartz cup and calcinated in a furnace at a temperature of 760°C in order to remove any remaining water and hydroxide.

Following the preparation of the ^{236}U into in oxide form, several issues arose surrounding the analysis of ^{236}U via AMS. There were two primary issues encountered during AMS operations that needed to be overcome in order to achieve reliable results.

The first issue was the abnormal behaviour of the samples themselves during AMS operation. When running the uranium oxide standards several large spikes of current and counts occurred during the measurements (Figure 12 A), when a relatively steady count rate was expected. Normally, the number of counts of an isotope would be observed gradually increasing over time as more of the sample is consumed before reaching a maximum, slowly decreasing as the sample is exhausted (Figure 12 B). When dealing with low concentration samples like those in the Arctic, a large spike of counts could severely impact results.

It is believed that the cause of these spikes is related to a sudden burst of ions from the material of the target. Until recently, uranium oxide samples were measured in a stainless steel

target, which is a poor heat conductor. At the high operating temperatures resulting from the analysis of uranium, the stainless steel target pieces were unable to dissipate the heat effectively. The buildup of heat eventually would lead to a small explosion in the sample, releasing a burst of sample material into the AMS beam line resulting in the observed spikes. This is not ideal as such an explosion and concentrated burst could waste the already small amount of sample material available, create particles with a wider range of energies, and potentially overwhelm the detector, lowering the number of ions counted as they pass through it. To resolve this issue, copper target pieces are now used for uranium samples. The copper target is a much better conductor and therefore better at dissipating heat buildup in the sample. This simple change in target material has removed the issue of the spikes in the count rates.

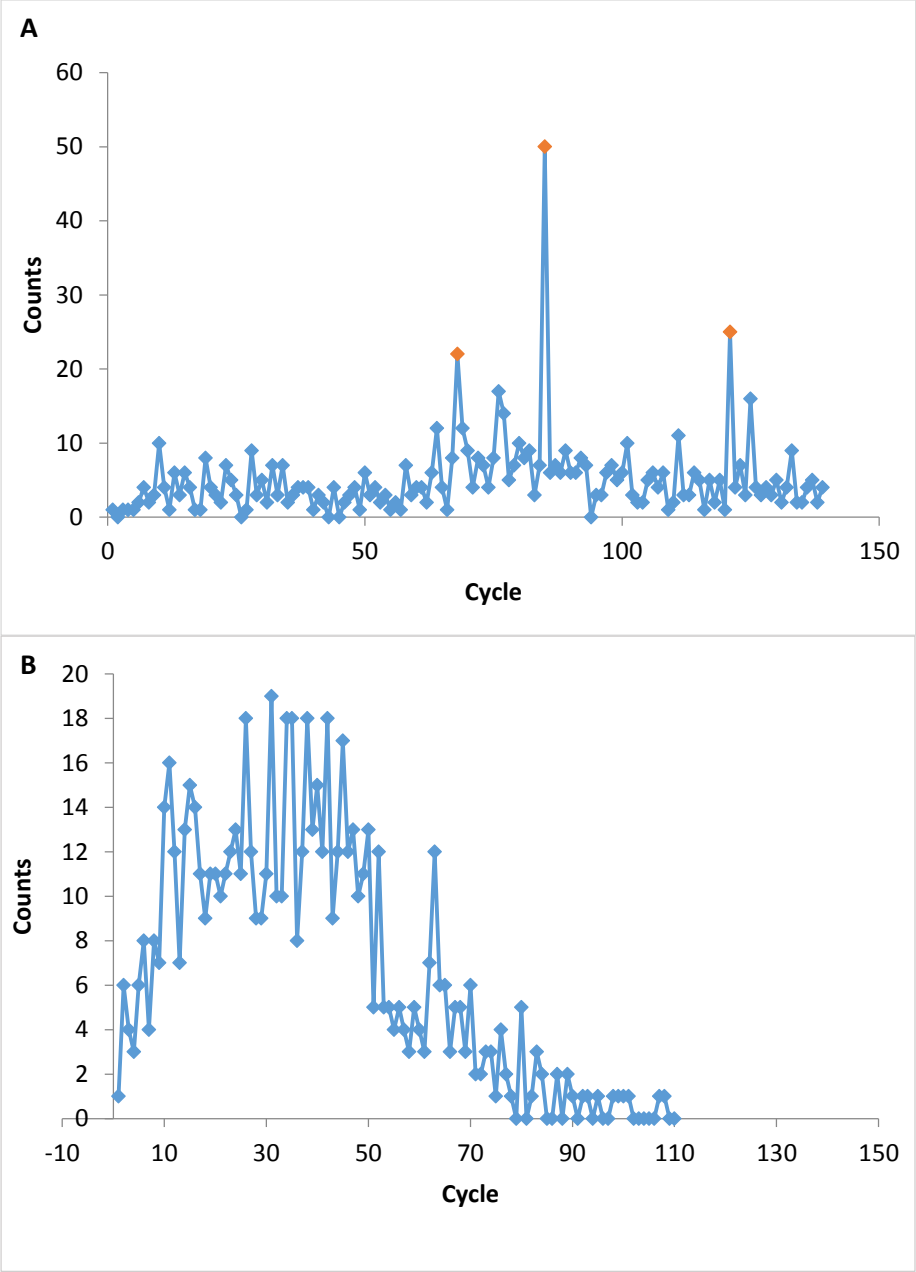

Figure 12: AMS data of counts per cycle of ^{236}U, figure A shows questionable behaviour with large spikes (orange points), while figure B shows a more ideal behaviour where counts increase over time.

The second issue was a bias observed in the initial measurements of the isotopes of uranium; specifically the ^{233}U yield tracer and ^{236}U. After creating and running a series of standards containing known amounts of both ^{233}U and ^{236}U with a constant concentration of ^{233}U and decreasing concentration of ^{236}U, it was found that the measurements showed a bias towards ^{233}U (Figure 13). It is believed that this issue arose from the positioning of the slits along the flight path of the ions within the spectrometer. The slits are metal plates at the focal points of magnetic of electric analysers that can be inserted or withdrawn to either increase the resolution or increase the acceptance of the analyser; blocking the path of undesired particles while allowing others to pass through. However due to the small mass difference between ^{236}U and ^{233}U, it is possible that the slits blocked some of the ^{236}U ions from reaching the detector therefore increasing the $^{233}U/^{236}U$ ratio. By determining slit settings that gave equivalent transmission for both isotopes the bias was eliminated, resulting in much more replicable results and the observed uranium isotope atom ratios agreed with the expected standards.

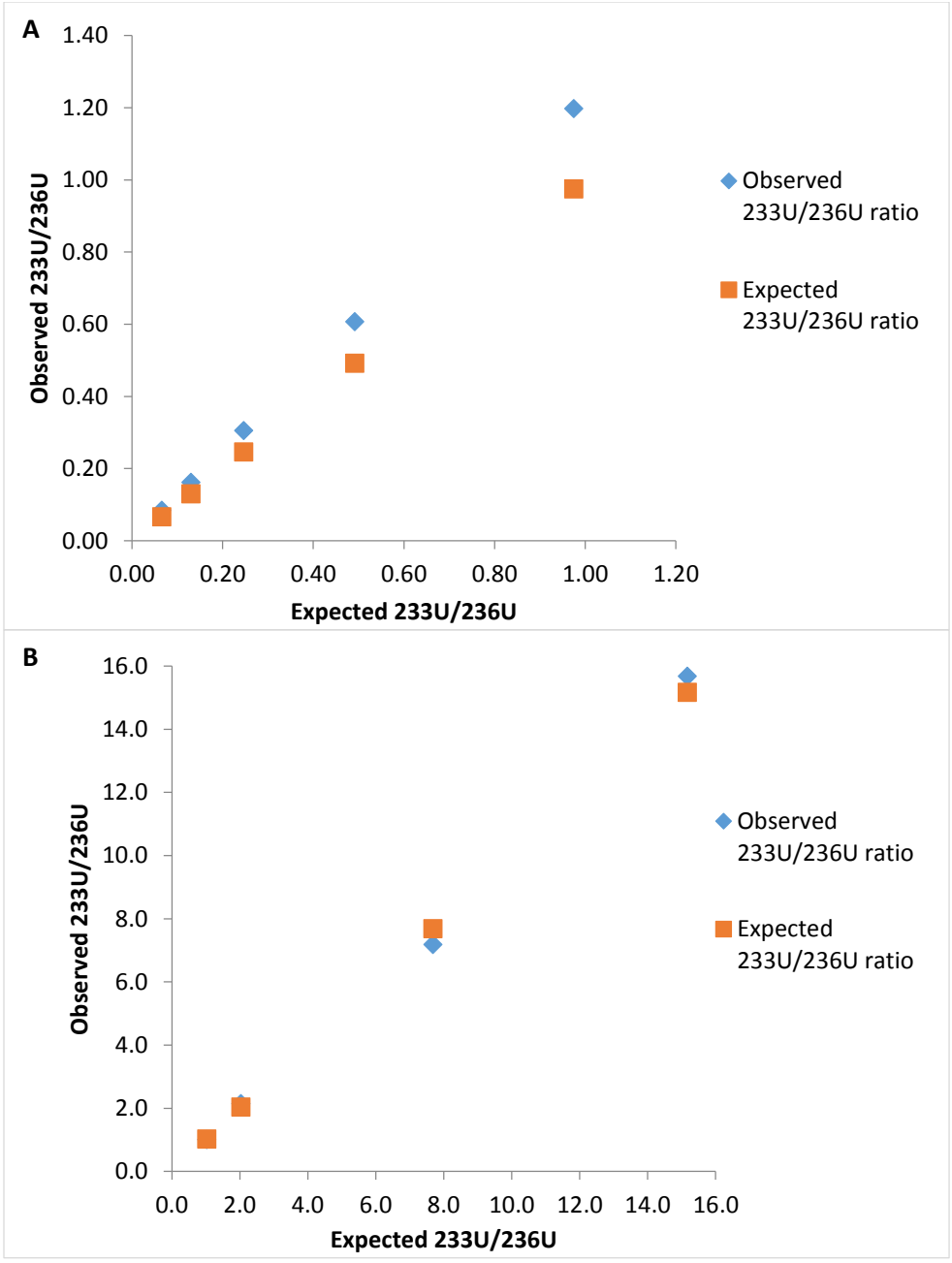

Figure 13: A: First expected vs. observed results of known ratios of $^{233}U/^{236}U$ from the AMS, B: Most recent expected vs. observed results of the same standards

2.5 Results and Discussion

^{129}I

Among the surface samples for ^{129}I from the Labrador Sea, there were interesting but not entirely unexpected trends across the AR7W line, with increased concentrations closer to both the Greenland and Labrador coasts and with lower concentrations located towards the centre of the Labrador Sea. The highest concentration was located at station 26 with a concentration of $2.33x10^{9}$ atoms/L of ^{129}I closer to the Greenland coast while the lowest value was $3.38x10^{8}$ atoms/L at station 13 closer to the centre of the Labrador Sea (Figure 14). These values fall well within the expected values for water labelled with ^{129}I discharge from the reprocessing plants in Europe. What is most likely being observed in Figure 14 is the West Greenland Current (WGC) flowing up the Greenland coast along with the returning Labrador Current along the Labrador coast (Figure 9) which has a slightly lower ^{129}I concentration due to splitting of the WGC in the Davis Strait with some ^{129}I labelled water continuing northward into the Arctic Ocean. Furthermore the returning Labrador Sea water is mixed with water exiting the Arctic Ocean via the Canadian Arctic Archipelago, consisting primarily of Pacific mixed layer water from the Arctic, which contains lower concentrations of radioisotopes, thus diluting the ^{129}I concentration in the Labrador Current derived from the WGC. The lower concentrations located in the central Labrador Sea are explained by the Labrador Gyre which undergoes relatively slow mixing with the encircling currents of the WGC and LC (Figure 9).

Figure 15A - 15C show a ^{129}I concentration/depth profile measured in 2014 at Station #17 compared with an ^{129}I profile from 2012 (15A), a temperature/depth profile (15B), and a salinity/depth profile (15C). As is evident from the figure, the surface waters show a slightly elevated concentration of ^{129}I. The concentration decreases gradually to a minimum at about

2040 m and then the ^{129}I increases consistently with increasing depth before reaching its maximum concentration ($1.04x10^{9}$) at 3670 m. Temperature at this station almost exhibits directly inverse behaviour to that of ^{129}I concentration as a function of increasing depth. While water temperature is slightly elevated in the surface and close to uniform up to 1500 m, it reaches a maximum at 2040 m before decreasing to its lowest value (1.8°C) at 3670 m. Salinity at this station exhibits a different trend with salinity increasing from between 1300 m and 2040 m where it also reaches its maximum. Salinity remained mainly uniform below this maximum except for a sharp decrease with increasing water depth near the bottom.

Figure 15 defines the different water masses present in the Labrador Sea based on their oceanographic characteristics as well as the concentration of ^{129}I. Combining these parameters simplifies the description of the different water masses. Beneath the surface layer lies the LSW which is defined by the uniform ^{129}I, salinity, and temperature between 500 and 1500 m. As mentioned above, this layer is well mixed during the winter due to its unique formation process, which results in its uniform composition. Directly beneath the LSW lies NEADW defined by its increased salinity and temperature, but it still contains ^{129}I concentrations similar to that of the overlying LSW. This makes sense in respect of NEADW's primary source, ISOW; which is formed in the waters between Iceland and Scotland, external to the primary transport route of tracer labelled water, the Norwegian Coastal Current. Finally, the deepest portion of the water column is dominated by DSOW defined by colder, lower salinity water having the highest concentrations of ^{129}I. DSOW is formed primarily from returning Atlantic water flowing southward along the eastern coast of Greenland in the East Greenland Current (EGC). The DSOW is colder and fresher, as it is formed primarily from modified Atlantic water returning from the Arctic which had originated in the northward flowing Norwegian Coastal Current. The

DSOW can therefore be defined not only by its low temperature and decreased salinity, but by the increased concentration of anthropogenic tracers from European nuclear fuel reprocessing plants such as ^{129}I. It is possible to discern the DSOW in Figure 15 at water depths below 3000 m from the salinity decrease in the transition between the NEADW and DSOW as well as from the increasing concentration of ^{129}I.

Figure 16 shows the depth profile of station 24 which is located closer to the Greenland coast. Figures A, B, and C show the ^{129}I concentration with depth, a comparison of temperature and ^{129}I concentration, and Salinity and ^{129}I concentration respectively. At station 24 the highest concentration of ^{129}I is at the surface and it slowly decreases with depth until reaching 1500 m before slowly increasing in concentration until reaching the deepest point. Temperature shows cooler temperatures at the surface before increasing by almost 3°C at 500 m. After reaching its temperature maximum at 500 m the temperature steadily decreases with depth until reaching the deepest point. Perhaps the most interesting in this figure is the salinity value, which after increasing to approximately 34.9 at 500 m is nearly unchanged with depth for the remainder of the column. This near steady salinity along with the weak trend in increasing ^{129}I concentration with depth when compared to station 17 implies that this close to the Greenland Coast there is little to no stratification of the different layers at station 17, apart from the difference in the surface waters and those at 500 m and downwards. At station 24 the highest concentration of ^{129}I is found in the surface waters and this agrees with the trend of increasing ^{129}I until reaching station 26 (Figure 14) which is a possible indicator of where the West Greenland Current lay in the spring of 2014. Following this line of reasoning, station 24 most likely lay within or on the edge of the West Greenland current, which can account for the lack of stratified layers at the station. The massive movement of water northwards stopped any clear pattern from developing.

Looking at the salinity profile of station 24, from 500 m onwards the water is quite uniformly mixed. We do see a slight increase of ^{129}I with depth but nowhere near as pronounced as that in station 17. However, similar trends are observed in ^{129}I concentration at both stations with depth until past the 3000 m mark. It is possible that due to the fact that station 24 is shallower than station 17 the increase in ^{129}I is not observed as there is not as much available space in the water column for the DSOW, and were both stations of similar depth the same trends may have been observed.

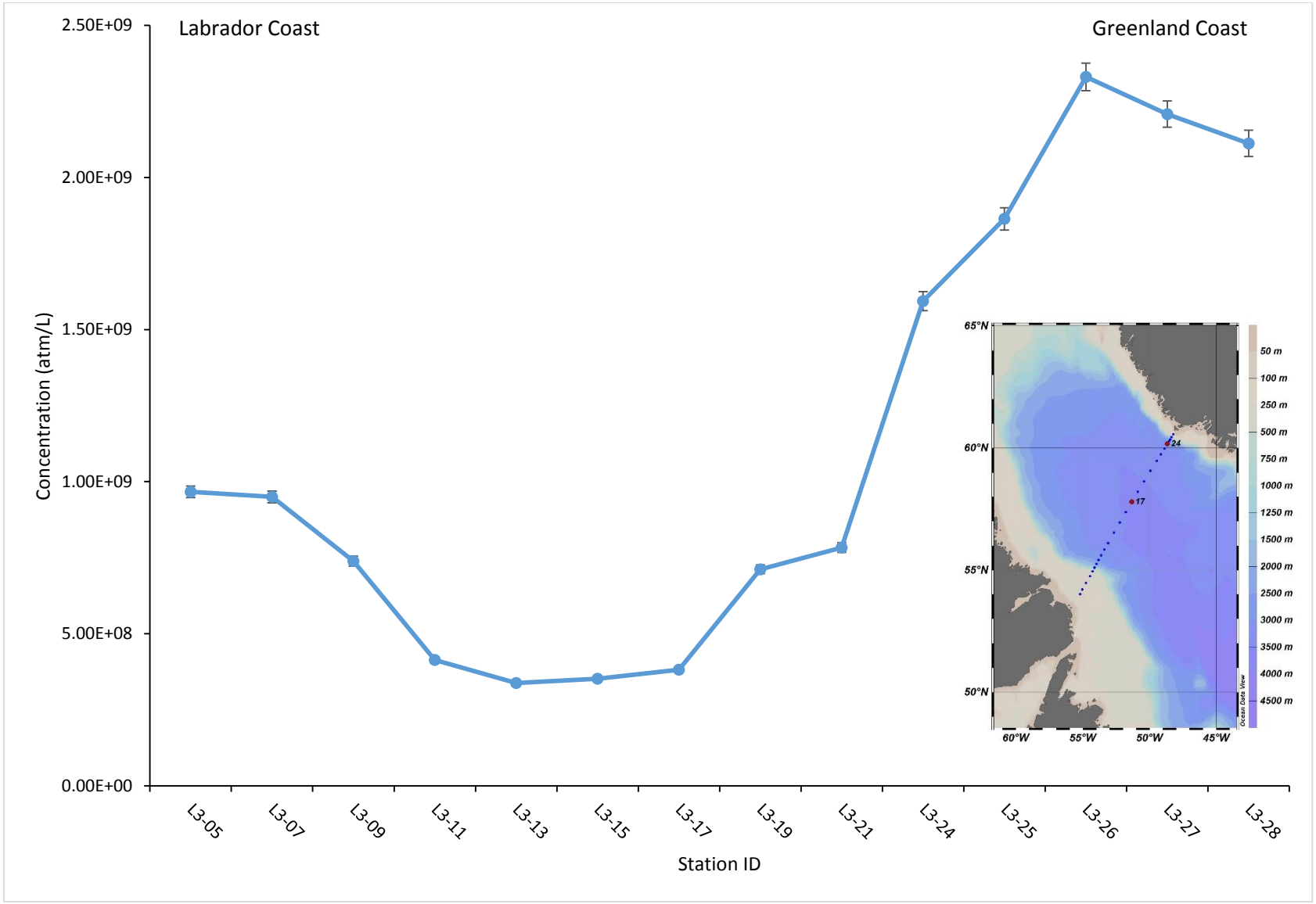

Figure 14: ^{129}I *concentration of surfaces waters across the AR7W Line in the Labrador Sea. Inset is the map of the transect and station locations.*

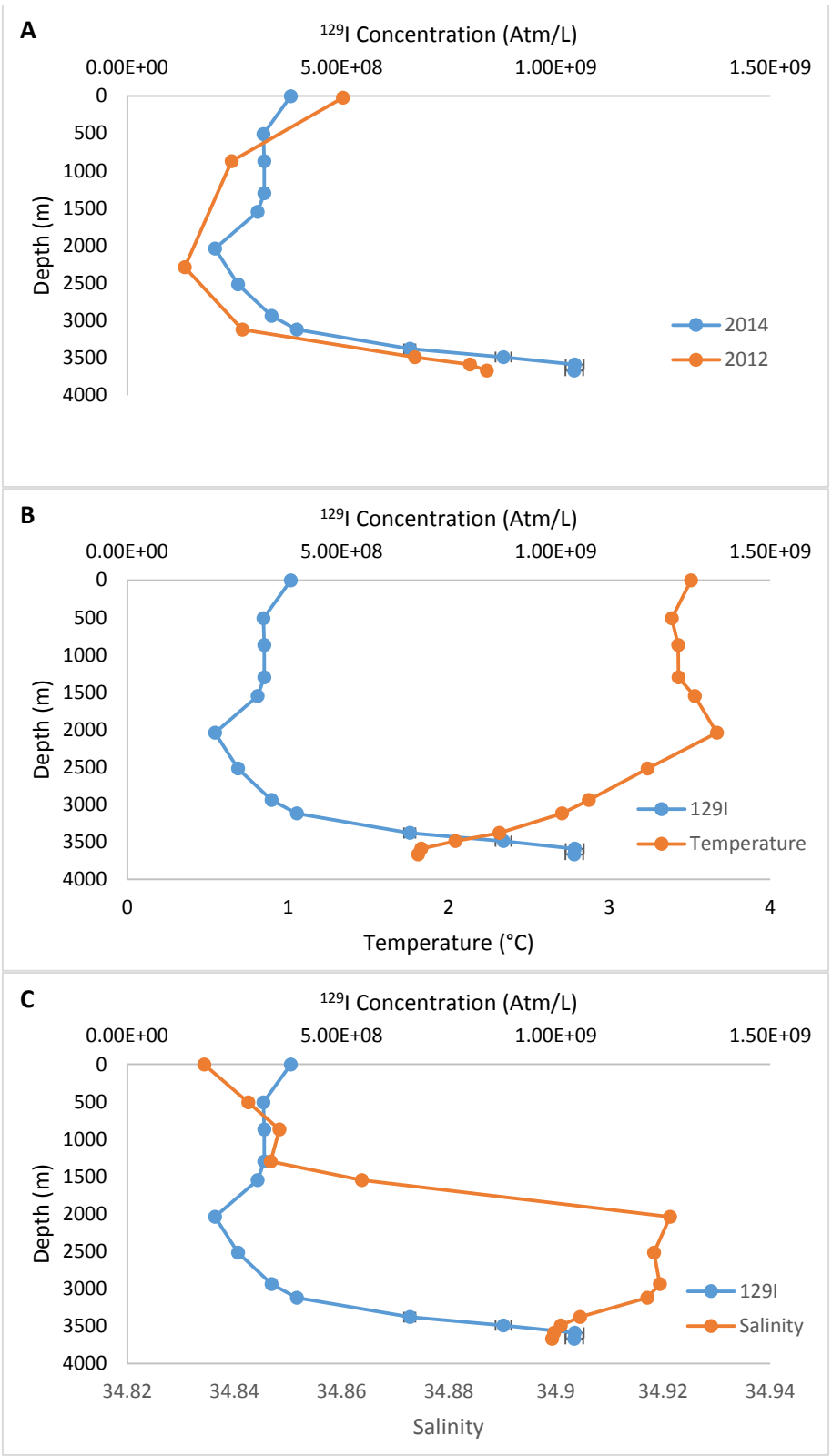

Figure 15:^{129}I Depth Profile of Station 17; Figure A shows a comparison between 2012 and 2014 ^{129}I values, Figure B is a comparison between ^{129}I concentrations and temperature with depth, while figure C is a comparison of ^{129}I concentration and salinity with depth

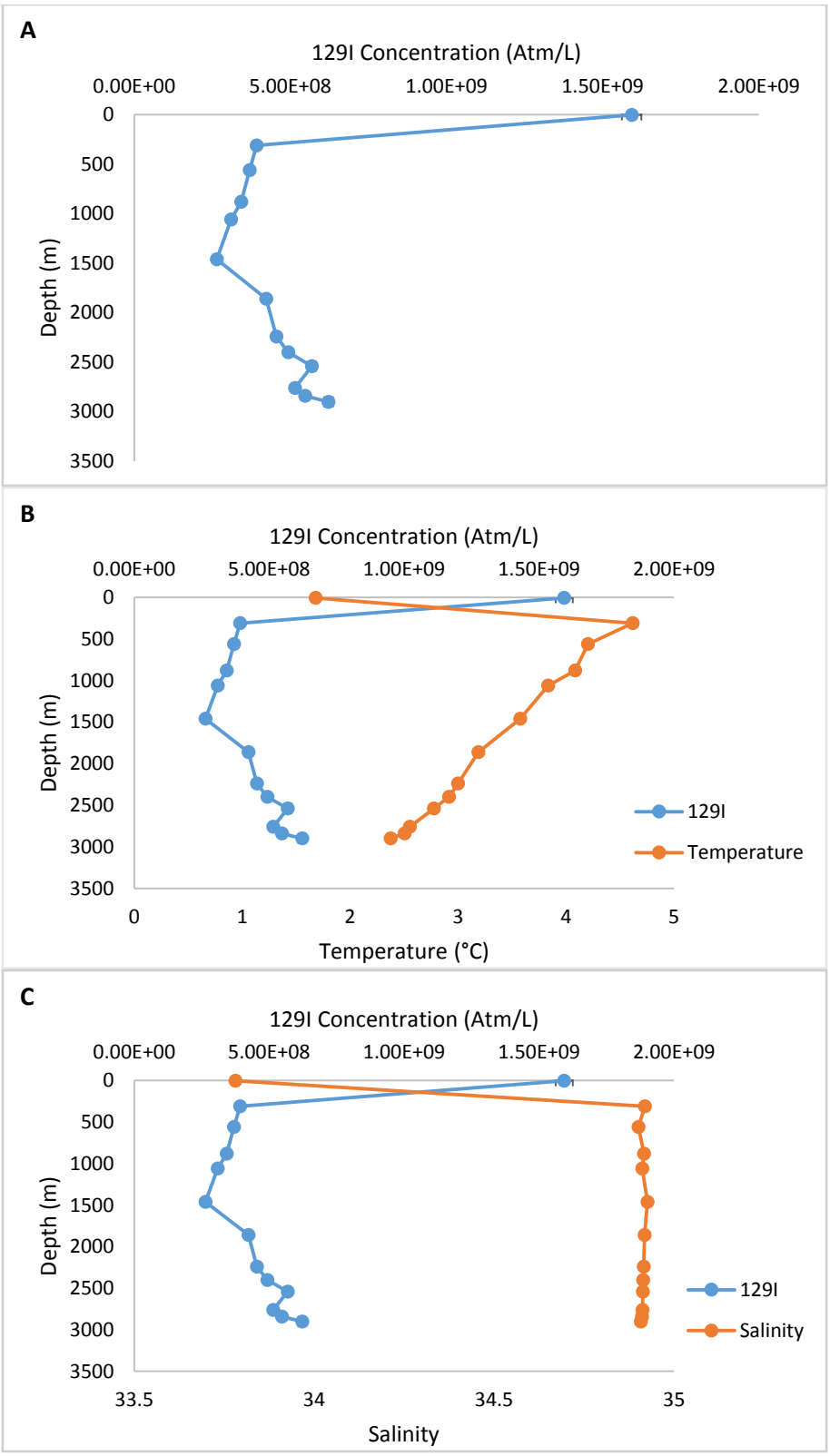

Figure 16: ^{129}I Depth Profile of Station 24; Figure A shows the concentration of ^{129}I with depth values, Figure B is a comparison between ^{129}I concentrations and temperature with depth, while figure C is a comparison of ^{129}I concentration and salinity with depth

^{137}Cs

^{137}Cs results from samples collected across the surface of the AR7W section are reported below in Figure 17. 137Cs concentrations vary by less than 1 Bq/m^3 across the entire transect. This is in agreement with fallout levels measured in the Arctic Ocean that were similar to those observed in the surface waters of the Labrador Sea (Smith et al., 2011). This is in agreement with the observed discharges of ^{137}Cs from the reprocessing plants which has decreased to almost 0 in the years since 1986 (Figure 6).

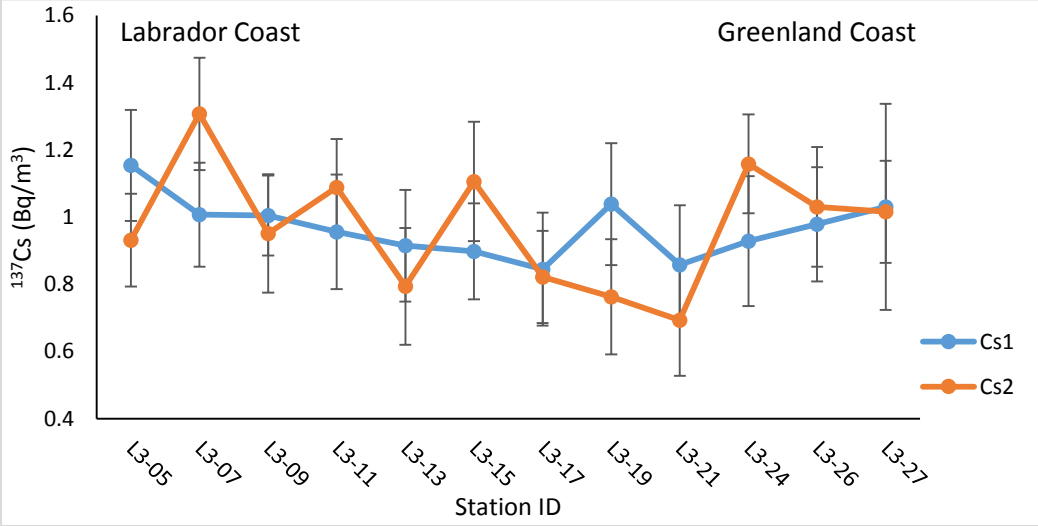

Figure 17: ^{137}Cs values across the surface of the Labrador Sea, Cs1 and 2 refer to duplicates taken at each station

^{236}U

Among the surface samples taken across the Labrador Sea, a trend nearly opposite to that of ^{129}I was observed in the distribution of ^{236}U concentrations. It was predicted that ^{236}U would follow a distribution similar to that of ^{129}I with higher concentrations closer to the coasts of the Labrador Sea because both isotopes have similar sources and behave conservatively in the ocean (Raisbeck et al., 1995; Sakaguchi et al., 2011). However, ^{236}U concentrations in the surface waters of the Labrador Sea do not match the trend of ^{129}I (Figure 18A). The highest values are actually located closer to the centre of the Labrador Sea, rather than within the outer boundary currents.

To ensure that this was not due to experimental error samples from selected stations were reanalysed (Figure 18B). There is little difference in the 236U values between runs 1 and 2, although analytical uncertainties were greater for the run 2 measurements. This uncertainty is due to the fact that limited sample material was available for run 2 and this reflected in the poorer counting statistics. However even with the large error associated with run 2, both runs show the same overall trend in the distribution of ^{236}U across the surface of the Labrador Sea.

^{236}U concentration ranged from 7.87×10^5 and 8.55×10^6 atoms/L., and although these values do not follow the expected distribution, they do agree with values measured previously in other areas of the other areas of the North Atlantic (Casacuberta et al., 2014; Christl et al., 2013). The ^{236}U concentration in the Denmark Strait ranges from 7.99×10^6 to 1.12×10^7 atoms/L (Casacuberta et al., 2014). These values are expected to be somewhat higher compared to those in the Labrador Sea due to their closer proximity to the reprocessing plants. ^{236}U values in the North Sea range from 6.10×10^6 to 1.67×10^8 (Christl et al., 2013). These ^{236}U levels are again higher than those in the Labrador Sea due to the proximity to the reprocessing plants. The

maximum ^{236}U value reported for the North Sea is directly downstream of the La Hague reprocessing plant in the English Channel.

^{236}U concentrations in samples collected in the Sea of Japan in 2010 show a range between $1.3x10^{6}$ to $1.6x10^{7}$ atoms/L (Sakaguchi et al., 2012), which is similar to the concentration range in the Atlantic Ocean. It is unlikely however that this similarity in concentration can be attributed to reprocessing plant input. An alternate explanation is the disproportionately large amount of atomic weapons testing that took place in the Pacific Ocean during the previous century. American weapons tests mainly occurred in the US Marshall Islands, depositing large amounts of isotopes such as ^{236}U locally. The fallout was then carried up into the Sea of Japan by the North Equatorial, Kuroshio and Tsushima currents (Sakaguchi et al., 2015) resulting in levels higher than those expected from global fallout.

The $^{129}I/^{236}U$ ratio can also be used to identify the source of these radionuclides in sea water. The $^{129}I/^{236}U$ ratio differs in global weapons test fallout, reprocessing plant inputs and natural production in the atmosphere (Casacuberta et al., submitted to Earth and Planetary Sciences). The distribution of the $^{129}I/^{236}U$ ratio, is closer to what would be expected (Figure 19) with higher values closer to the coasts, and the ratio of isotopes observed is from reprocessing plants. Observing such a high $^{129}I/^{236}U$ ratio confirms the influence of reprocessing plants, while lower values indicate a higher influence from global fallout (Casacuberta et al., submitted to Earth and Planetary Sciences). New research into the use of $^{236}U/^{238}U$ and $^{129}I/^{236}U$ as a dual tracer has shown that higher values in both imply the presence of reprocessing plant water while a $^{236}U/^{238}U$ ratio between $1x10^{-9}$ and $4x10^{-9}$ and a $^{129}I/^{236}U$ ratio close to 0 implies influence from global fallout (Casacuberta et al., submitted to Earth and Planetary Sciences). Comparing Figure

20 and Figure 21, the majority of ^{236}U in the Labrador Sea surface waters are a combination of both Global Fallout and reprocessing plant origins.

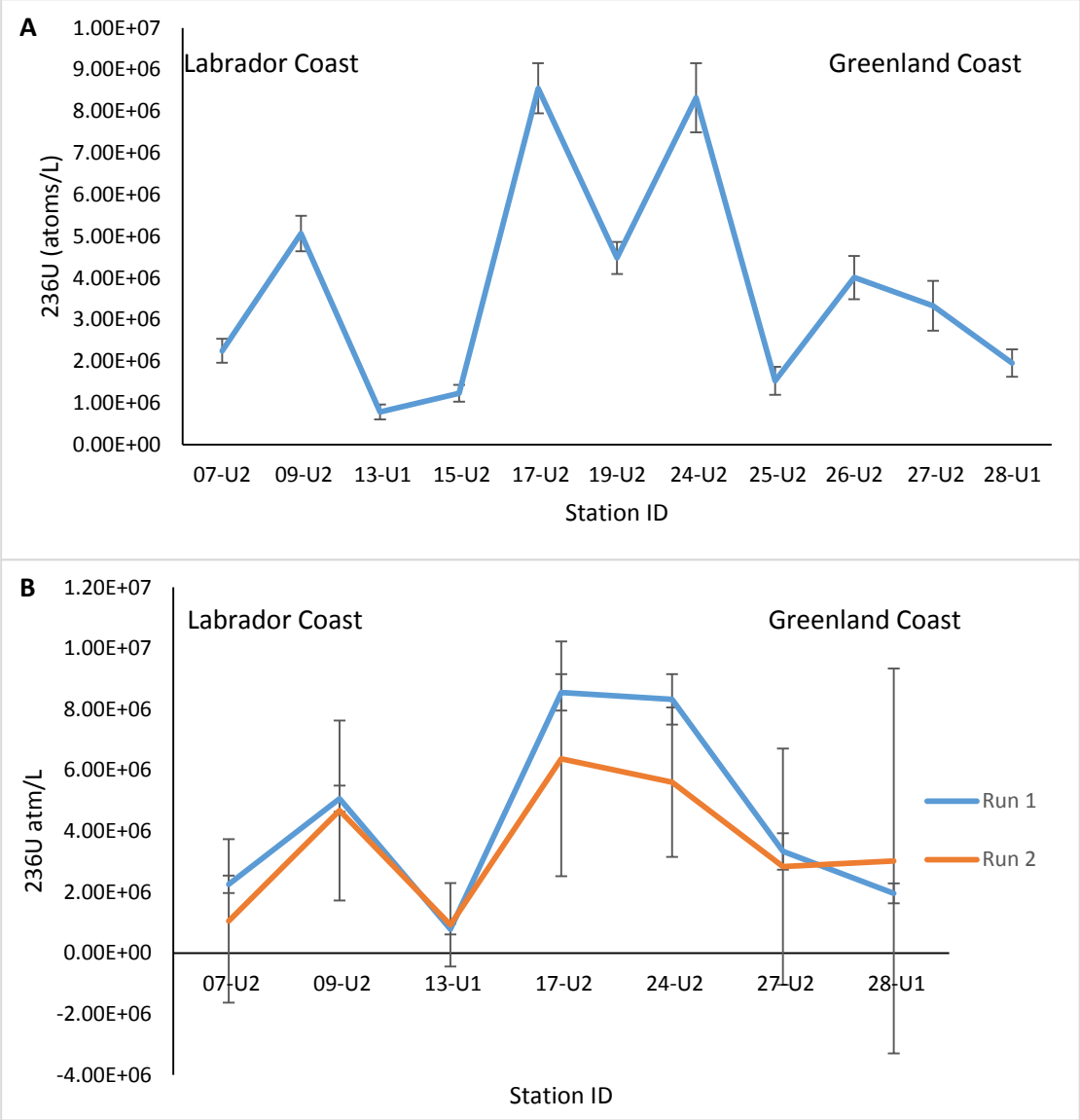

Figure 18: A: Run 1 ^{236}U concentrations across surface waters of the Labrador Sea, B: comparison between Run 1 and 2 for select stations across the Labrador Sea.

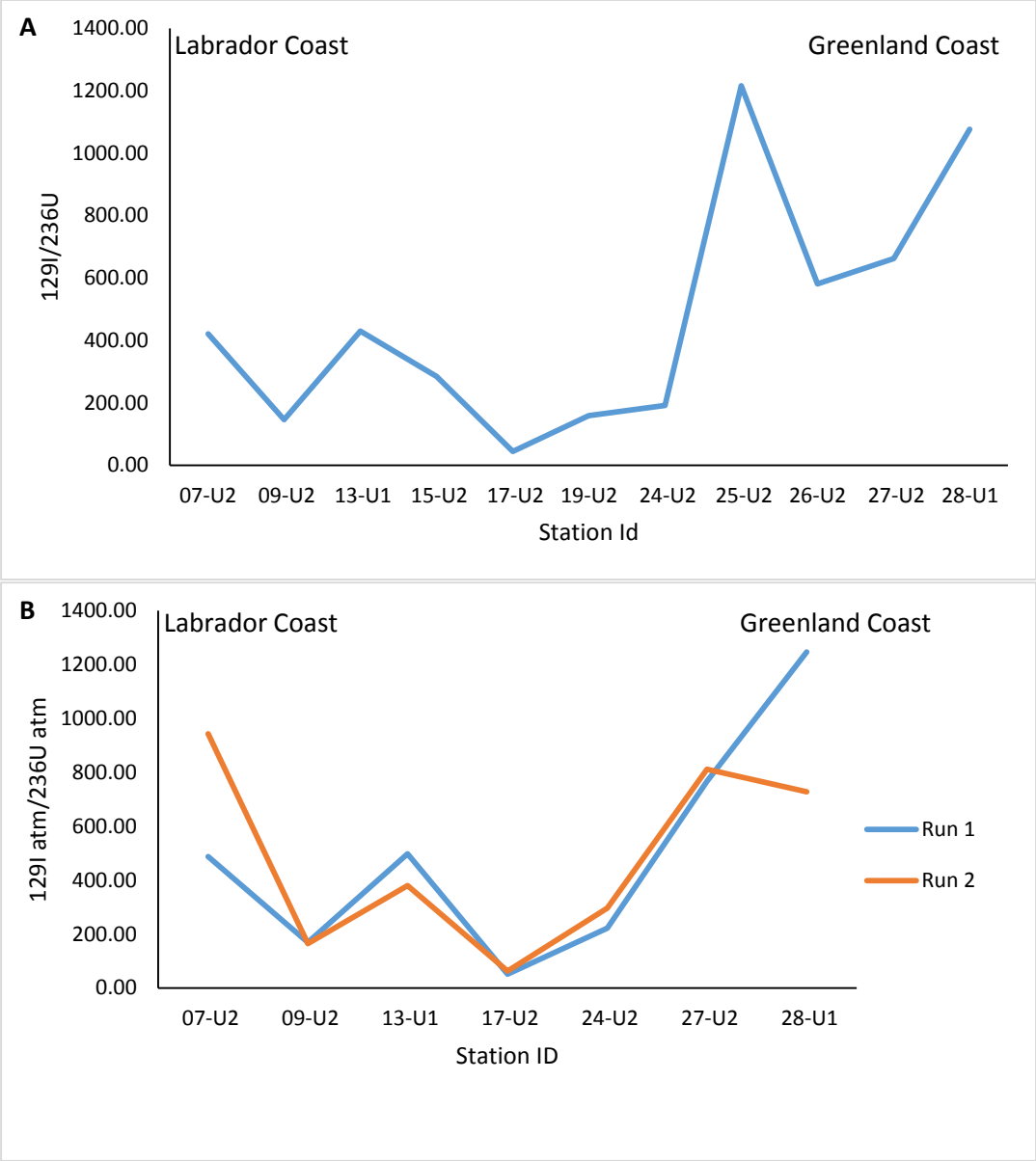

Figure 19: A: $^{129}I/^{236}U$ distribution across the Surface waters of the Labrador Sea, B: comparison between run 1 and 2 of $^{129}I/^{236}U$ distribution across the Labrador Sea

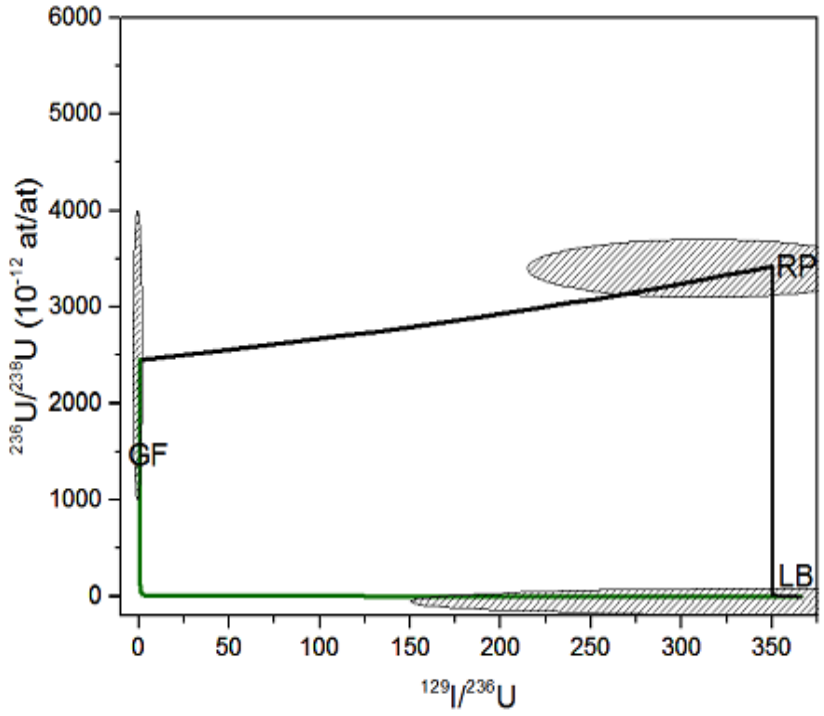

Figure 20: Sources of ^{236}U based on $^{129}I/^{236}U$ ratios and $^{236}U/^{238}U$ ratios, GF is global fallout, RP is reprocessing plant, and LB is lithogenic background (Casacuberta et al., submitted to Earth and Planetary Sciences)

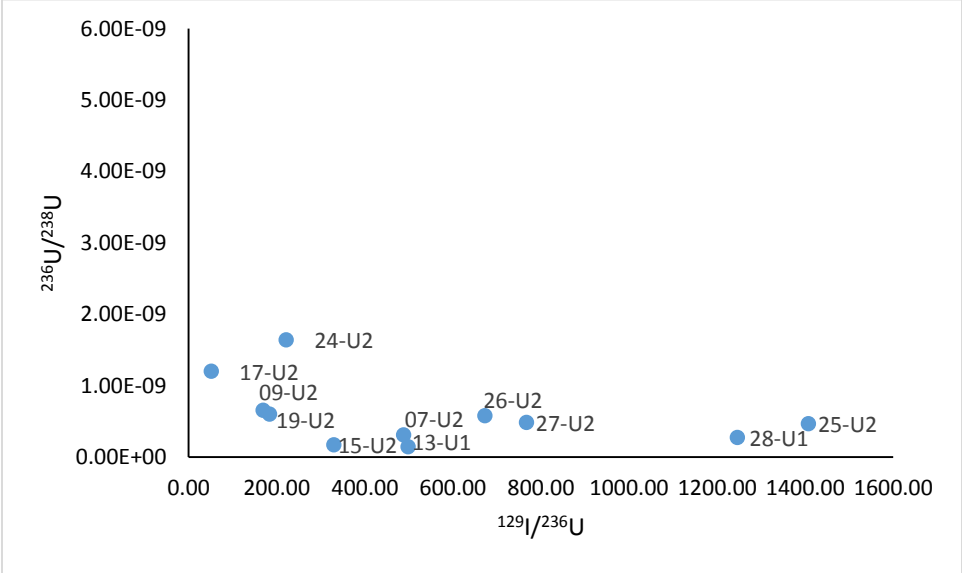

Figure 21: Distribution of $^{129}I/^{236}U$ ratios and $^{236}U/^{238}U$ ratios at stations across the Labrador Sea (add red box to show inset)

3. The Arctic Ocean

The Arctic Ocean is a strongly stratified and enclosed sea consisting of two major basins and multiple shallow shelves with only four passages connecting it to the World's Oceans (Rudels et al., 1994). The Barents Sea, Fram Strait, and Canadian Arctic Archipelago connect the Arctic Ocean to the North Atlantic, while the Bering Strait is the Arctic Ocean's sole connection to the Pacific Ocean (Rudels et al., 1994). 53% of the Arctic Ocean is characterized by large shallow shelves such as those of the Barents (200-300 m deep), Kara (50-100 m), Laptev (<50 m), and East Siberian (<50 m), and Chukchi Seas (50-100 m;Rudels, 2009) The two large basins which make up the deepest points of the Arctic Ocean are the Eurasian and Canadian Basins which are separated by the Lomonosov Ridge. The Eurasian Basin can be further subdivided into the Nansen and Amundsen basins, separated by the Gakkel Ridge, while the Canadian Basin can be subdivided by the Alpha and Mendeleyev Ridges into the Makarov and Canada Basins (Rudels, 2009).

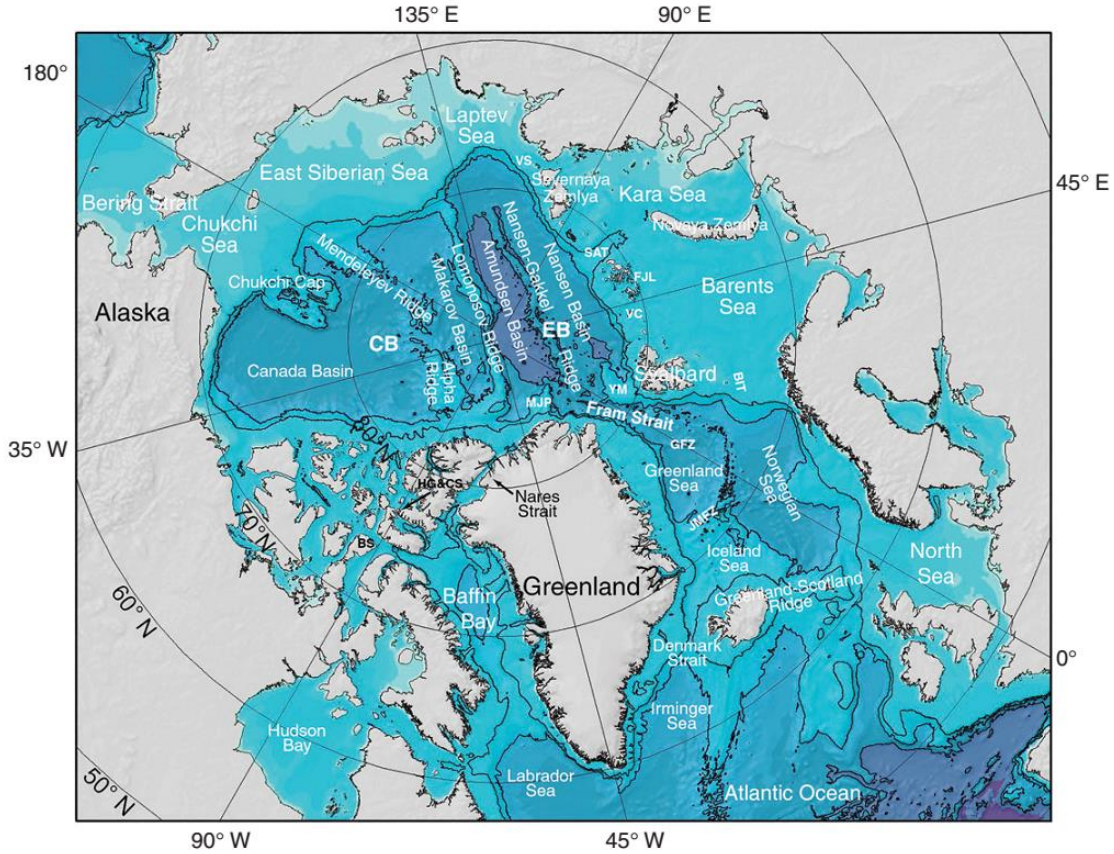

Figure 22: Map of the Arctic Ocean showing geographical and bathymetric features. The bathymetry is from IBCAO (the International Bathymetric Chart of the Arctic Ocean; Jakobsson et al., 2000; 2008) and the projection is Lambert equal area. The 500 and 2000 m isobaths are shown. All maps used here are made by Martin Jakobsson). BIT, Bear Island Trough; CB, Canadian Basin; EB, Eurasian Basin; GFZ, Greenland Fracture Zone; MJP, Morris Jessup Plateau; JMFZ, Jan Mayen Fracture Zone; SAT, St. Anna Trough; YM, Yermak Plateau; VC, Victoria Channel; VS, Vilkiltskij Strait; FJL, Franz Josef Land; BS, Barrow Strait; HG & CS, Hell Gate and Cardigan Sound. (From Rudels, 2009)

3.1 Arctic Ocean Water Masses

While climate change driven warming of the Arctic, as well as sea ice loss are important issues and arguably the most well-known challenges regarding the environmental stability in the Arctic, they make up only a small part of a complex and important natural system, with many variables involved. One such variable is the circulation of water throughout the Arctic and its ultimate fate. The Arctic Ocean is comprised of several different water layers having unique characteristics. In oceanography, water masses are most simply distinguished by their temperature, and salinity measured in parts per thousand.

The majority of water enters the Arctic from two sources in the North Atlantic: the Barents Sea and through the Fram Strait located between Greenland and the island of Svalbard (Jones, 2001). A much smaller input (approximately 10% of the total) occurs from the Pacific Ocean through the shallow (depth < 50 m) Bering Strait between Russia and Alaska (Jones, 2001). Upon entering the Arctic several changes occur resulting in the formation of distinct layers of water. The upper 50 m of the Arctic Ocean is referred to as the Polar Mixed Layer (PML), dominated mainly by surface temperatures governed by atmospheric cooling and sea ice production and fed mostly by river runoff, melted sea ice, and water entering from the North Atlantic and Pacific Oceans (Rudels, 2009). The PML is homogenized during the winter by freezing, brine release and haline convection, while during the summer months it becomes freshened from melting sea ice (Rudels, 2015). The salinity ranges from 30 to 32.5 in the Canadian basin, and 32 to 34 in the Eurasian Basin (Rudels, 2009). Below the PML is a halocline which separates it from the rest of the water column (Jones, 2001; Rudels, 2009).

The halocline is characterised by temperatures close to 0°C, and a very steep density gradient associated with the increasing salinity with depth (Rudels, 2015). In the western Arctic the halocline is steepened by the inflow of Pacific water, which is less dense than the underlying Atlantic Layer (Rudels, 2015). This water layer occupied the 100-250 m depth range and is characterized by increasing salinity from 32.5 to 34.5.

The warmer water of the North Atlantic entering the Arctic Ocean through Fram Strait encounters sea ice which causes partial melting, thereby freshening the surrounding water and forming a halocline (Jones, 2001; Rudels et al., 1996) Warmer (2 – 3 °C) and denser water entering the Arctic Ocean from the North Atlantic form the Atlantic Layer (also referred to as intermediate waters) of the Arctic Ocean (Jones, 2001) at water depths of 400 – 900 m and with salinity ranging from 34.5 to 35 (Figure 24).

The deepest layer of water is Arctic Deep Water (ADW) which includes inputs from both the Bering Strait and Barents Sea. During winter in the Barents Sea temperatures decrease which encourages the formation of sea ice, causing the surrounding water to increase in salinity. The increase in salinity is such that it increases the water density enough for it to flow off the shelf in plumes to the depth of Arctic Deep Water (Jones, 2001) which in turn results in salinity increases to around 34.94. A similar process can occur with water entering through the Bering Strait, where increased salinity from sea ice formation injects water into the Arctic Deep layer.

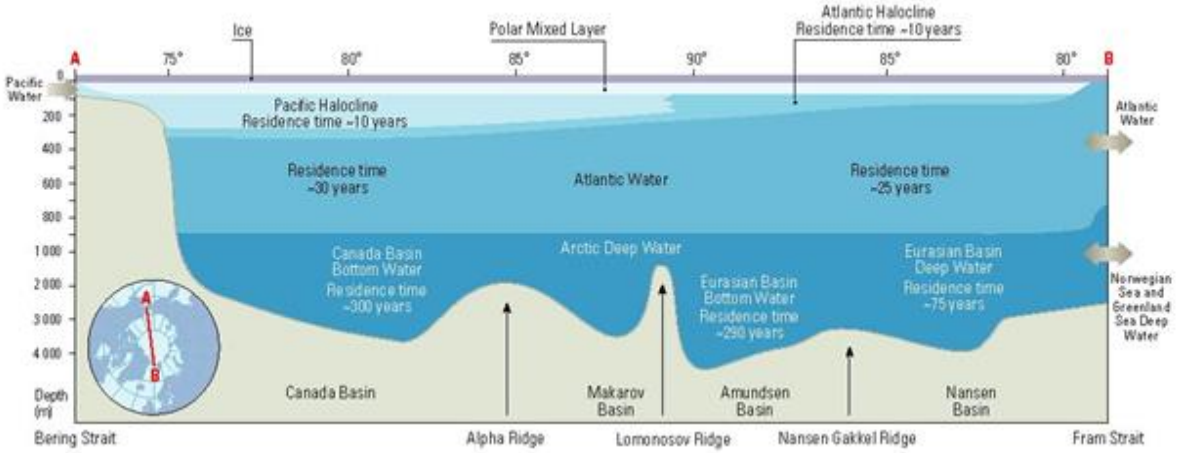

Figure 23: Major water masses of the Arctic (AMAP, 1998)

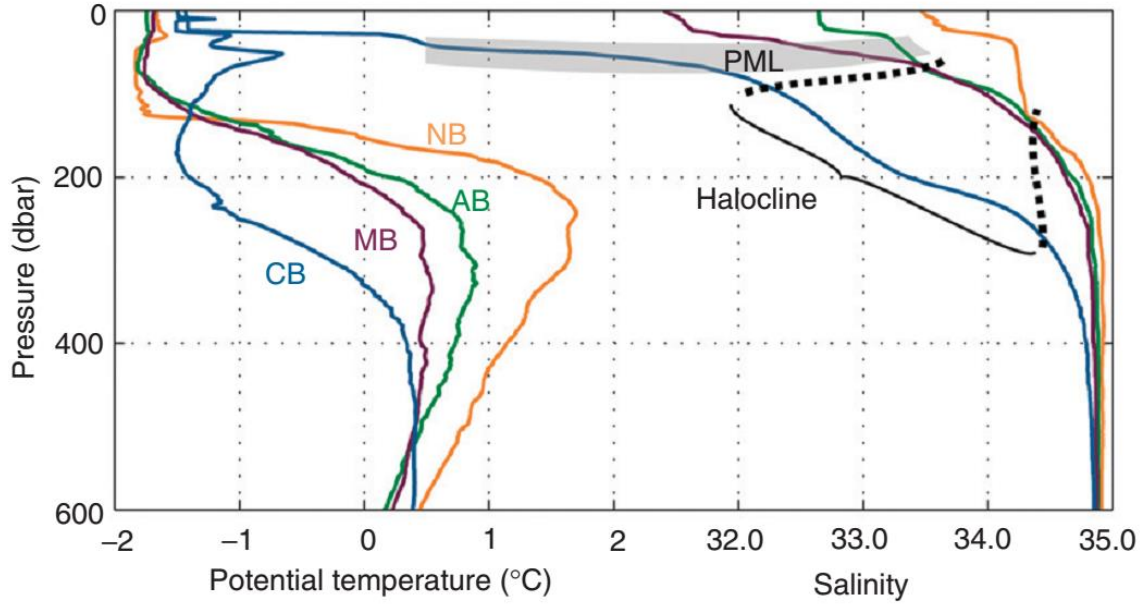

Figure 24: Temperature and Salinity Depth profiles of the Canadian Basin (CB, Blue), Makarov Basin (MB, Magenta), Amundsen Basin (AM, Green), and Nansen Basin (NB, Yellow) (Rudels, 2009) (1dbar = 1.01m)

3.2 Arctic Ocean Circulation

The movement of the aforementioned water bodies in the Arctic is also an important component of the region. Due to the variability in external forces such as temperature and wind, as well as the differences in the water masses themselves, it is not as simple as having each layer behave identically. The portion of the PML entering from the North Atlantic generally follows an eastern route until hitting the Lomonosov ridge. It then flows along the ridge before returning to exit through the Fram Strait (Jones, 2001). PML formed from Pacific water entering from the Bering Strait splits in the Chukchi sea, with one half flowing along the North American coast while the other flows north to eventually mix with water from the Atlantic Layer before exiting through the Canadian Arctic Archipelago and the Fram Strait (Jones, 2001). As this layer is closest to the surface it is influenced partially by local wind, however the Pacific Ocean possesses a higher sea level than the Arctic Ocean. This in turn causes a pressure gradient to develop in the Bering Strait, pushing water into the Arctic Ocean (Rudels, 2009).

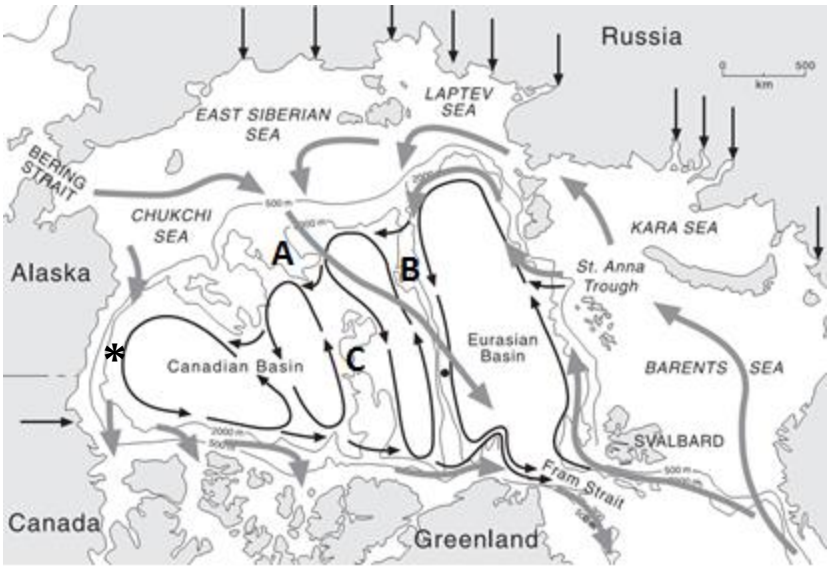

Figure 25: Arctic Circulatory Patterns of Surface water (grey arrows), and Atlantic Layer and Upper Polar Deep water to around 1700 m (Black arrows) Straight black arrows represent major rivers. The letters refer to major subsurface ridges where A is the Mendeleyev Ridge, B is the Lomonosov Ridge, C is the Alpha Ridge, the asterisk shows the approximate location of Station A. Adapted from Jones, 2001

Below the PML, the Atlantic layer and the upper portion of the Polar Deep Water follow completely different circulation patterns (Figure 25). Warmer Atlantic water is carried

Northwards by the Norwegian Atlantic Current, where it then splits into two. One flow enters into the Barents Sea before continuing into the Arctic, while the second body moves towards the Fram strait and enters the Arctic Ocean through it before continuing East along the bottom of the Nansen Basin in what is called Fram Strait Branch Water (FSBW) (Rudels, 2009; Karcher et al., 2012). The branch travelling through the Barents Sea can be split into two layers. The lighter Atlantic Water which is cooled and freshened from interactions by sea ice (Karcher et al., 2012; Rudels et al., 2004) experiences mixing from river runoff and is responsible for feeding the surface water of the Eurasian Basin before gradually recirculating towards the Fram Strait (Karcher et al., 2012). The second branch is the denser portion of Barents Sea Atlantic Water which enters into the Nansen basin as Barents Sea Branch Water (BSBW) where there is limited mixing between it and the FSBW. The BSBW and FSBW flow cyclonically around the Arctic Ocean in the boundary current which splits at each of the major ridges (Rudesl, 2009). One loop enters the Makarov basin along the Mendeleyev Ridge, while another enters into the Canadian Basin at the Chukchi plateau. The boundary current carrying intermediate Atlantic Water also enters into the Canada basin at the Alpha ridge and the Makarov Basin from the Lomonosov ridge (Rudels, 2009; Karcher et al., 2012). These general circulation patterns can be observed in Figure 4 and Figure 25. Interestingly, these distinct gyres introduce a time lag that makes the Atlantic waters entering these basins distinct, even if they originated from the same inflow into the Arctic Ocean (Rudels, 2009)

3.3 Beaufort Sea Sampling Methods

Samples were taken across the Beaufort Sea with depth profiles for Iodine being taken at each station, while Uranium and Cesium depth profiles were taken at Station A. Station locations can be viewed below in Figure 26.

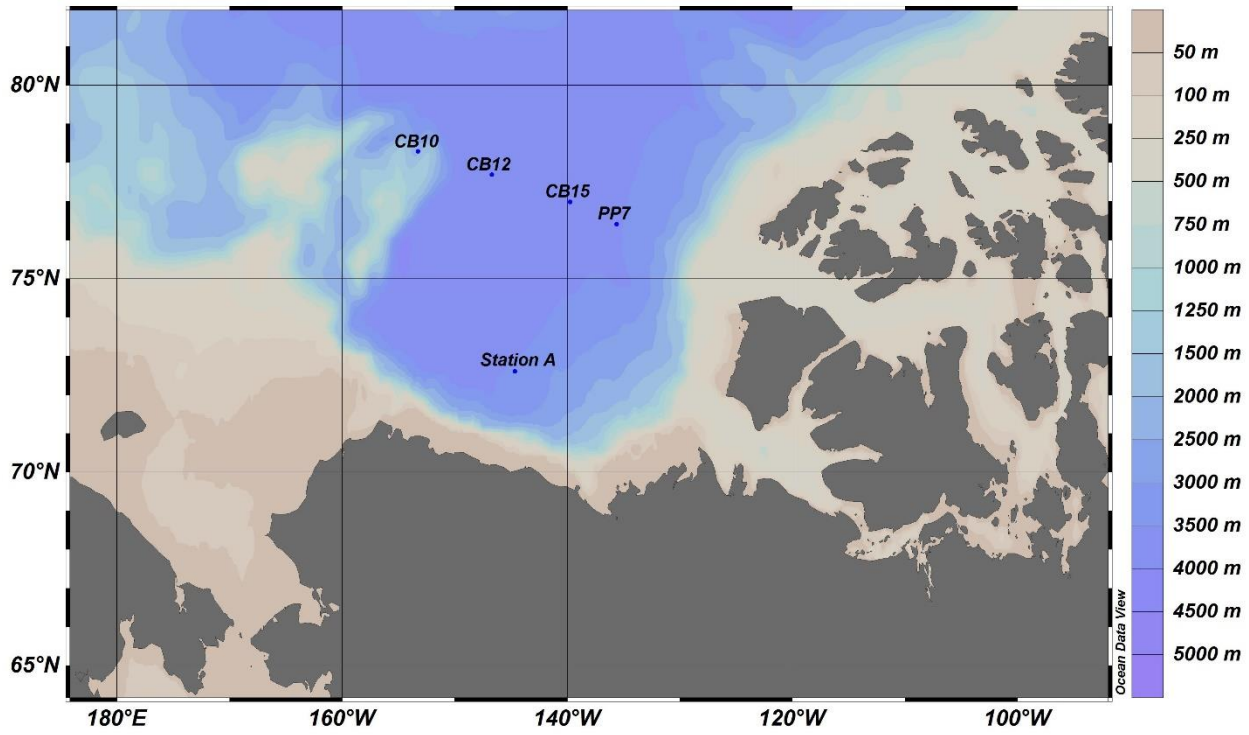

Figure 26: Beaufort Sea sample locations and station ID's

Table 2: Samples taken at each station in the Beaufort Sea by depth in metres

Station A	CB10	CB12	CB15	PP7
6m	4m	5m	7m	6m
202m	174m	187m	180m	180m
307m	269m	451m	454m	451m
358m	444m	510m	509m	510m
404m	510m	612m	611m	612m
510m	611m	814m	814m	814m
607m	815m	1016m	1017m	1017m
806m	1017m	2034m	2034m	2035m
1013m		3684m	3591m	3427m
2035m				
3293m				

^{129}I

The method for collection of ^{129}I remained unchanged to that of the samples taken in the Labrador Sea. A sample list can be viewed above in Table 2

^{137}Cs

The method for the collection of ^{137}Cs remained unchanged. However due to an error in the calculation of the spike solution 100 nanograms of ^{133}Cs spike was added to the samples in the Beaufort Sea rather than 100 micrograms. Furthermore, ^{137}Cs samples from Station A were run twice on two different gamma detectors to ensure reproducibility. The gamma detectors possess different parameters and the intercomparison between them is discussed below. The two detectors are the CANBERA SAGe detector, and the ORTEC HPGe detector. The CANBERA detector contains thicker shielding than the ORTEC, which is more effective at blocking incoming external radiation, and also possesses a larger and thicker germanium crystal which is more effective at detecting gamma radiation from samples. Due to these differences the CANBERA detector has an efficiency approximately double that of the CANBERA. Furthermore both detectors were calibrated independently using two different methods. The ORTEC detector was calibrated traditionally by measuring a standard of known concentration and geometry and generating a calibration curve. The CANBERA detector was calibrated with a Monte Carlo simulation based on the various components of the detector. By comparing the same samples on both independently calibrated detectors, and achieving similar results supports the validity of the data.

^{236}U

The method for collection of ^{236}U was modified with one additional step compared to the method in the Labrador Sea. After the addition of acid and the ^{233}U spike, 0.6ml of 12% Titanium Trichloride was added as a reducing agent to promote U^{4+} formation as it is less soluble than its U^{6+} form (Zavodska et al., 2008). It was found that upon returning to the lab and processing the uranium samples that the $TiCl_3$ was not removed and remained with the final precipitate, which made it difficult to work with. It would not be recommended to use $TiCl_3$ in the future as any potential benefit was outweighed by the trouble it caused in processing. Furthermore, due to limitations on available water, the supernatant used to acquire the cesium samples was recovered and reused for Uranium sampling.

3.4 Results and Discussion

^{129}I

Within the Beaufort Sea, ^{129}I samples (Figure 27) showed similar trends across all the stations sampled. At each station there is a strong trend of a sharp increase of temperature and ^{129}I concentration at approximately the 500 m mark followed by a rapid decrease in both temperature and ^{129}I concentration with depth. Among the deep stations (Station A, CB-12, CB-15, and PP7) ^{129}I concentration has decreased significantly by the time it reaches 2000 m and continues to decrease slightly by the bottom of the profile. Temperature across the deep stations behaves similarly as well, decreasing between 500 m and 2000 m before increasing slightly at the deepest point. A slight anomaly can be viewed at station A regarding the temperature difference between the surface point and the following point at 200 m. The other stations present express similar trends of approximately -1.5°C in the surface water and first 200 m before

increasing to the temperature maximum at 500 m, while Station A has a temperature maximum at the surface before decreasing rapidly to a value similar to that of the other stations at 200 m. This is most likely due to Station A's position further south as the air temperature became much colder further north. Another interesting trend is the apparent increase in temperature between the 2000 m and 3500 m point at all the deep stations sampled. One potential explanation is the increase in pressure with increasing depth, causing an increase in temperature. Another possible reason for the higher temperature is the location of the Lomonosov Ridge, which separates the Canadian basin from the other major Arctic basins. The location of this basin stops colder bottom waters located in the other basins from flowing into the Canada basin causing it to have a higher temperature in the bottom waters (Tomczak & Godfrey, 1994).

The ^{129}I trends observed in the Beaufort Sea data can be explained by the different water masses explained above. Relatively low concentrations of ^{129}I are observed in the surface waters as it is made primarily up of water originating from the Pacific Ocean as well as flow from river systems emptying into the Arctic Ocean, both low with anthropogenic tracers when compared to water labelled with discharge from the nuclear reprocessing plants of Europe. This also explains the lower salinity in the surface waters when compared to the rest of the profile. Melting sea ice, along with injections of fresh river water and less saline Pacific water reduces the salinity of the surface Arctic Ocean.

Increasing in depth it is possible to observe the Atlantic layer, identified by higher temperatures as well as the increased concentration of ^{129}I concentration. This again is due to the origins of this water entering the Arctic. The Atlantic water first passed through the British Isles and North Sea, becoming labelled with isotopes released from Sellafield and La Hague before continuing up the Norwegian Coastal Current through the Fram Strait and into the Arctic Ocean.

The rather rapid decline in ^{129}I concentration with depth after reaching its maximum is due to the entry into the Arctic Deep layer where; relative to the ^{129}I concentration maximum, values are close to 0. This is due to the extremely long residence time of the Artic Deep Layer of around 300 years, and of course, since the advent of the nuclear age is less than a century old, little to no anthropogenically produced radioisotopes have penetrated into this layer.

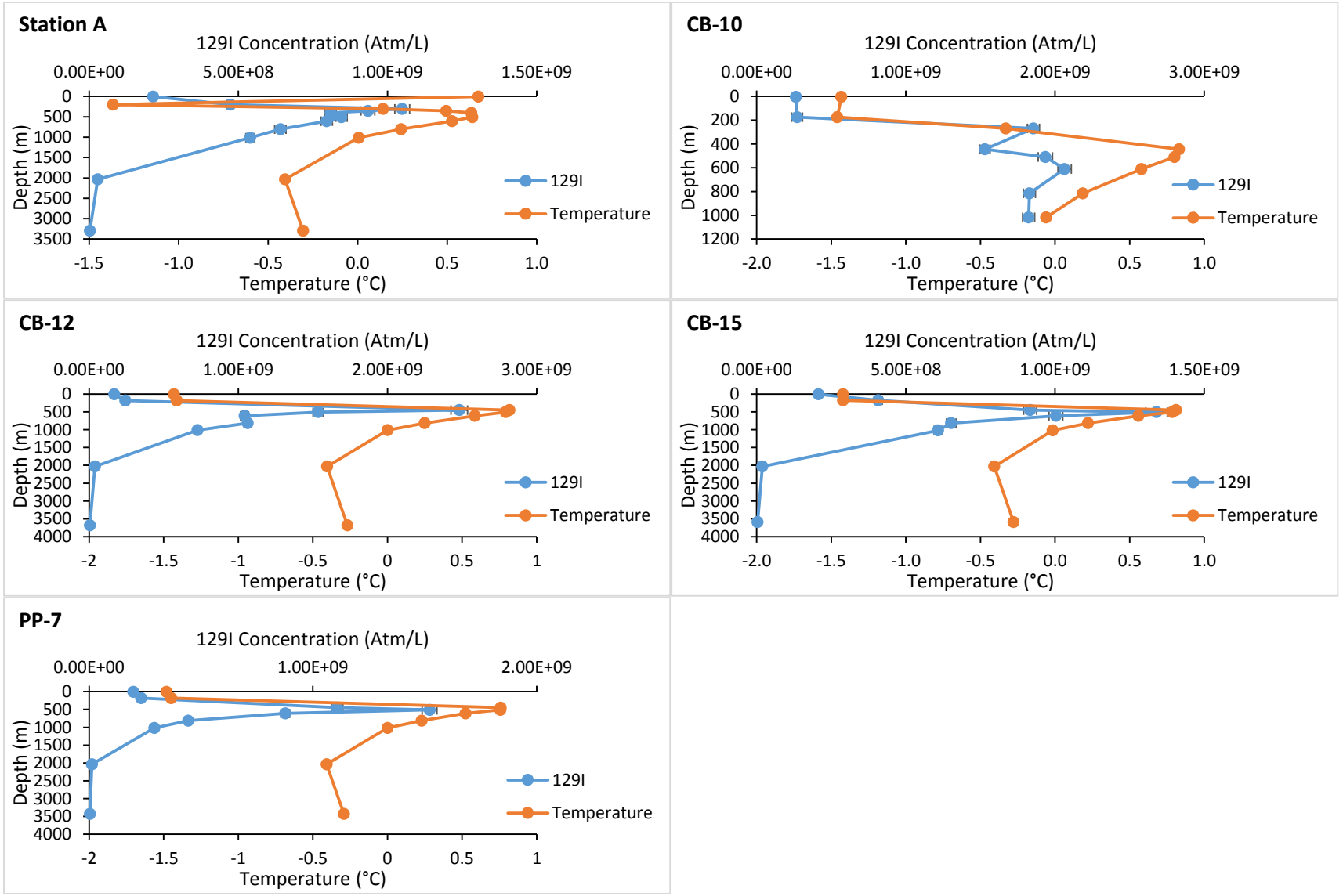

Figure 27: ^{129}I and Temperature depth profiles across the Beaufort Sea

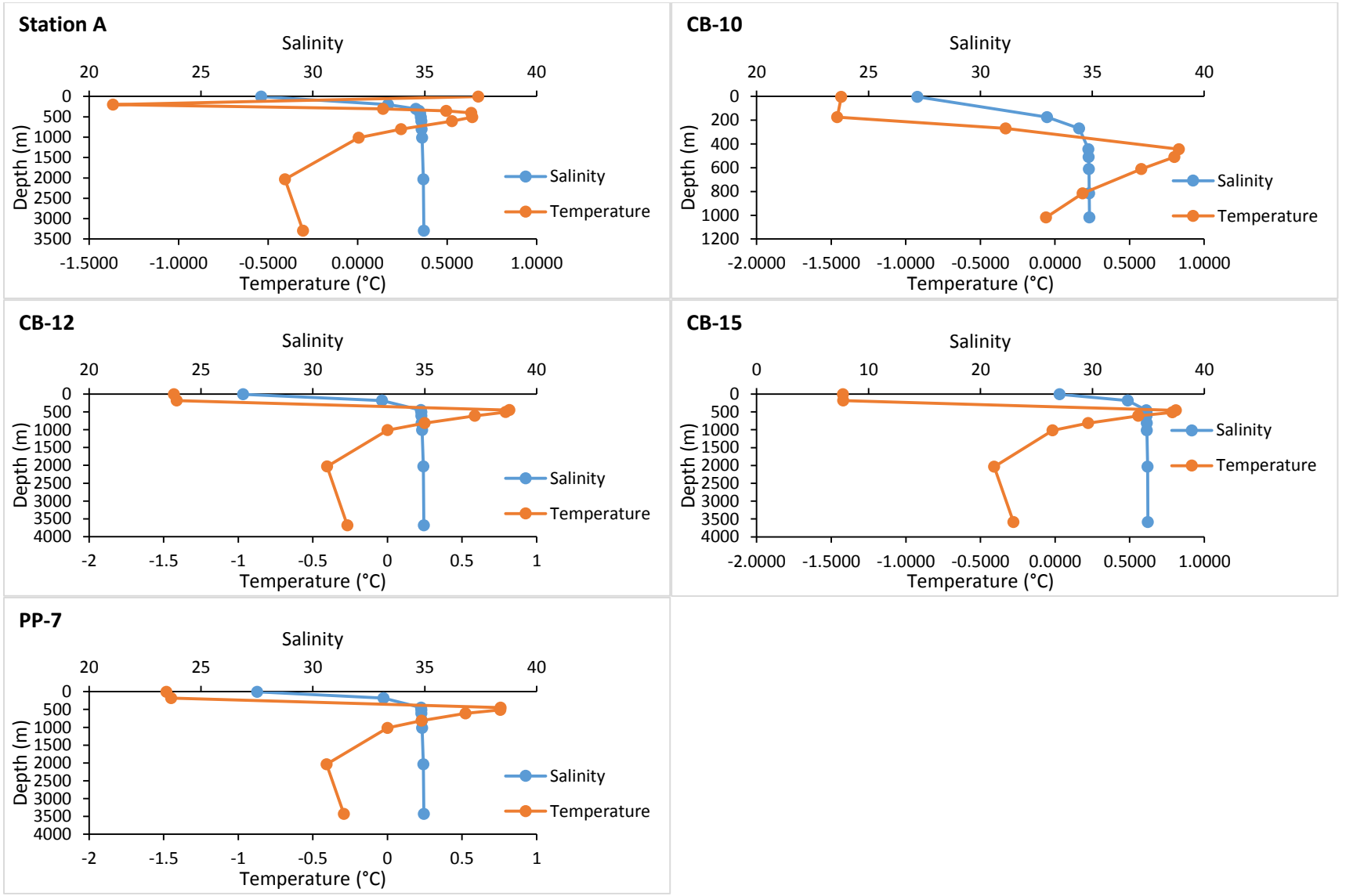

Figure 28: Salinity and Temperature depth profiles across the Beaufort Sea

^{137}Cs

^{137}Cs at Station A shares a nearly identical trend to that of ^{129}I above with values of approximately 1 Bq/m^3 in surface waters before increasing to a maximum concentration at 400 m, after which it slowly decreases with depth. The reason for this trend is the same as that for ^{129}I as tracer labelled Atlantic water occupies the mid depth at the concentration maximum before transitioning into the Deep Arctic layer. The concentration of $1Bq/m^3$ at the surface is expected for background fallout levels so there is little to no influence from the nuclear reprocessing plants in the upper 200 m of the water column consisting of the Pacific mixed layer and halocline. The low concentration maximum of only $2.5Bq/m^3$ is due to the small amount of ^{137}Cs being released by the nuclear reprocessing plants today. The transit time from the site of the nuclear reprocessing facilities to station A in the Canada basin was modelled to be approximately 14 years (Smith et al., 1998). This time period still falls within the period of low releases from the reprocessing plants. Furthermore, the residence time of the Atlantic layer in the Arctic is around 30 years which implies there may still be some ^{137}Cs present from the period of increased releases of ^{137}Cs as well as fallout from Chernobyl. It is therefore most likely that the majority of the ^{137}Cs in the Atlantic layer is indeed from reprocessing inputs, with a small contribution from other sources such as Chernobyl (Smith et al., 1998)

To ensure the reproducibility of the results, the depth profile of station A was run on two different gamma counters and their results were compared (Figure 29A) The difference between the two counters is that the CANBERA detector had a much larger germanium crystal and a thicker surrounding shield than the ORTEC counter resulting in double the counting efficiency. It is clear from the figure that the results are indeed reproducible with results from both counters overlapping their respective uncertainty. These results increase our confidence that these data

are an accurate representation of the depth distribution of ^{137}Cs at Station A.

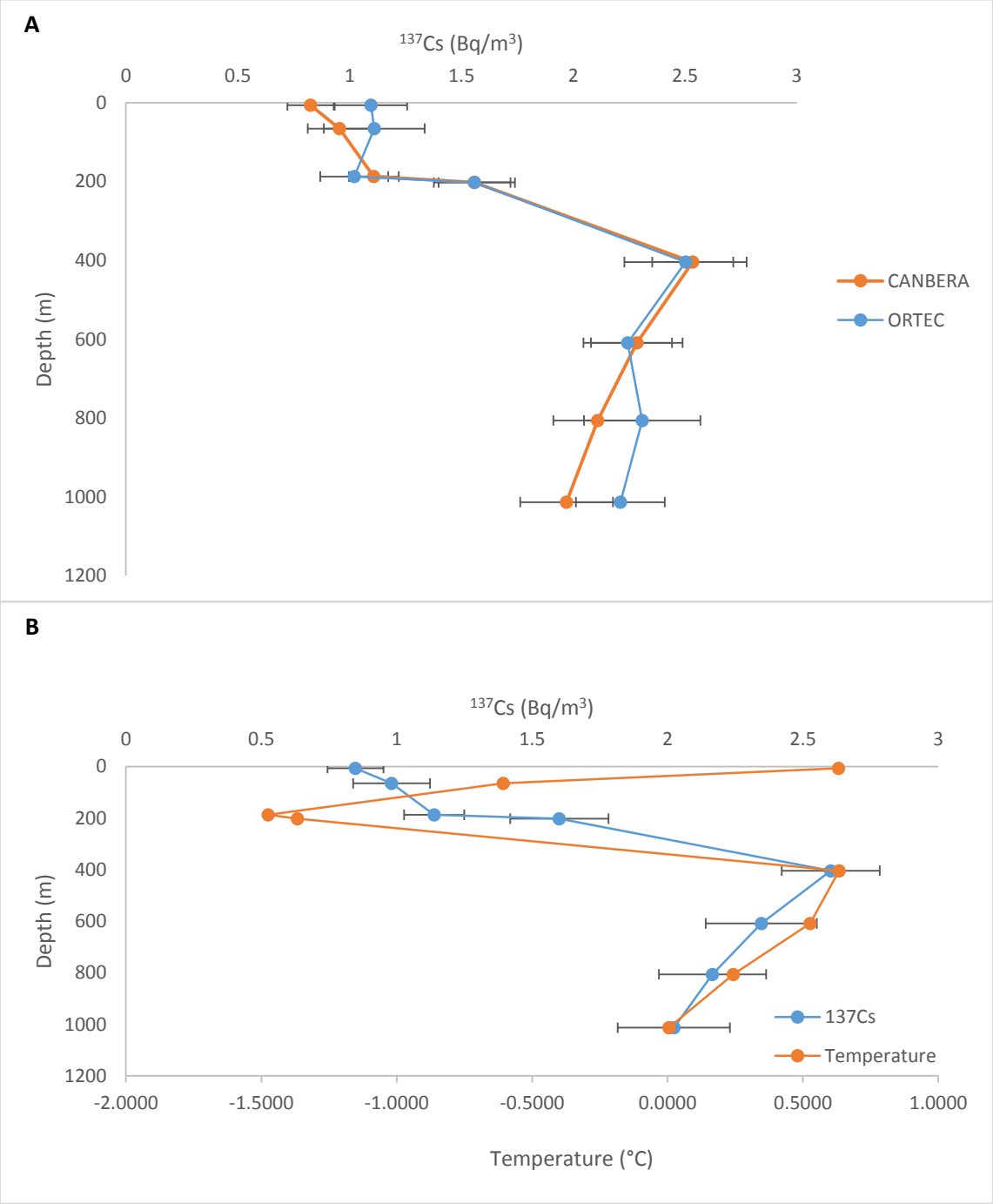

Figure 29: A: Comparison of ^{137}Cs values with depth between two different Gamma detectors at Station A. B: ^{137}Cs concentration and Temperature with depth at Station A

^{236}U

Concentration of ^{236}U measured in the Beaufort Sea ranged from $6.60x10^{9}$ to $8.31x10^{9}$ atoms/L and was relatively constant for the entirety of the depth profile. The calculated values can be found in Table 3. It is believed that these concentrations are not indicative of the actual concentration or distribution of ^{236}U in the Beaufort Sea. These concentrations are believed to be suspect for two reasons. First, the recorded concentrations of ^{236}U in the Beaufort Sea are higher even than those measured directly off the coast of the La Hague reprocessing plant which is higher than $1.67x10^{8}$ (Christl et al., 2013). Secondly, ^{236}U in the Beaufort Sea is also expected to follow a distribution similar to that of ^{129}I, but no such trend is observed. Instead ^{236}U maintains relatively unchanged concentration with depth. It is believed the high and uniform concentration is due to contamination from an outside source of ^{236}U. Given the nature of the uniform concentration in each sample this contamination could have been from one of the chemicals or materials added during the sampling process, although this is hard to believe since all the same materials were used in both the Labrador Sea and Beaufort Sea sample processing. The only difference in the Beaufort Sea was the addition of $TiCl_3$ and the reuse of water used in ^{137}Cs processing. Both of these differences were determined not to be able to have such a large impact on ^{236}U concentration. The current cause of ^{236}U concentration is therefore unknown.

Although the samples in the Beaufort Sea gave unsatisfactory oceanographic results they did help to confirm the reliability of the sampling and analytical process as the duplicates proved highly reproducible (Table 3). The high concentrations of ^{236}U also provided useful samples for the continued improvement of the A.E. Lalonde AMS methodology for ^{236}U measurement.

Table 3: ^{236}U concentration in atoms/L in the Beaufort Sea, values with the same depth are duplicates

Sample ID	Depth (m)	^{236}U atoms/L
U242	5	5.92E+09
U237	64	6.07E+09
U234-1	185	5.95E+09
U234-2	185	5.97E+09
U232	200	6.61E+09
U228-1	400	6.66E+09
U228-2	400	6.52E+09
U225-1	600	6.08E+09
U225-2	600	6.04E+09
U223	800	5.53E+09
U221-1	1000	7.16E+09
U221-2	1000	7.69E+09

4. Conclusions

This work measured ^{129}I, ^{137}Cs and ^{236}U in seawater from the Beaufort Sea, Arctic Ocean and the Labrador Sea. All three isotopes help to identify the origin of the water in different parts of the water mass.

The water in the Labrador Sea contains ^{129}I from reprocessing plants. In Labrador Sea surface water, the highest ^{129}I values were in the current circling the outer limit of the Labrador Sea, in the West Greenland Current and Labrador Current, with lower values towards the centre of the Labrador Sea in the Labrador Gyre. In the deeper waters, the highest ^{129}I values were observed at the greatest depth in the Denmark Strait Overflow Water, which originates from the Norwegian Coastal current. ^{129}I is a well-documented anthropogenic tracer and these values from the Labrador Sea are consistent with previous measures reported by Smith (2011). ^{137}Cs values in all of the surface waters of the Labrador Sea were close to global fallout levels of 1 Bq/m^3 and there is no evidence of elevated concentrations of ^{137}Cs from the reprocessing facilities.

^{236}U was successfully measured by AMS at the A.E. Lalonde Laboratory. Throughout the course of this research, the method for the analysis of ^{236}U was greatly improved. The concentrations of ^{236}U across the Labrador Sea are similar to those reported in the North Atlantic Ocean. The measured distribution of ^{236}U in the Labrador Sea did not follow the distribution predicted by the distribution of ^{129}I.

In the Beaufort Sea both ^{129}I and ^{137}Cs concentrations were very different in different water masses that are found in different depths in the Canada Basins. The depth

distributions of both isotopes are consistent with the distributions that were expected based on oceanographic data.

The samples for ^{236}U in the Beaufort Sea were unfortunately contaminated by a still unknown source. As a result, the distribution of ^{236}U in the Beaufort Sea could not be determined. However the ^{236}U results were highly reproducible lending credibility to the sampling and analytical method. Based on these results, it shows the potential for ^{236}U as a useful oceanographic tracer in terms of both sampling methodology as well as its analysis via AMS.

Future work should include depth profiles of stations in the Labrador Sea to observe the distribution of ^{137}Cs and ^{236}U with depth, paying special attention to the bottom 500 m. In the Beaufort Sea, four depth profiles for ^{129}I, ^{137}Cs, and ^{236}U were collected in September of 2015, but unfortunately were not able to be analyzed within the timeframe of this thesis. A higher resolution between the depths of 200 m to 600 m depth would allow for analysis of the expected maximum for the anthropogenic tracers within the Atlantic Layer.

5. References

AMAP, 1998. AMAP Assessment Report: Arctic Pollution Issues. Arctic Monitoring ai+nd Assessment Programme (AMAP), Oslo, Norway. xii+859 pp.

Anisimov, O.A., D.G. Vaughan, T.V. Callaghan, C. Furgal, H. Marchant, T.D. Prowse, H. Vilhjálmsson and J.E. Walsh, 2007: Polar regions (Arctic and Antarctic). Climate Change 2007: Impacts, Adaptation and Vulnerability. Contribution of Working Group II to the Fourth Assessment Report of the Intergovernmental Panel on Climate Change, M.L. Parry, O.F. Canziani, J.P. Palutikof, P.J. van der Linden and C.E. Hanson, Eds., Cambridge University Press, Cambridge, 653-685.

Casacuberta, N., Christl, M., Lachner, J., van der Loeff, M. R., Masqué, P., & Synal, H. -a. (2014). A first transect of 236U in the North Atlantic Ocean. *Geochimica et Cosmochimica Acta*, *133*, 34–46. doi:10.1016/j.gca.2014.02.012

Casacuberta, N., Masqué, P., Henderson, G., Rutgers van-der-Loeff, M., Bauch, D., Vockenhuber, C., Christl, M. (n.d.). First data of 236U in the Arctic Ocean and consequences of using 236U/238U and 129I/236U as a new dual tracer. Submitted to *Earth and Planetary Science*.

Chamizo, E., López-Lora, M., Villa, M., Casacuberta, N., López-Gutiérrez, J. M., & Pham, M. K. (2015). Analysis of 236U and plutonium isotopes, 239,240Pu, on the 1MV AMS system at the Centro Nacional de Aceleradores, as a potential tool in oceanography. *Nuclear Instruments and Methods in Physics Research Section B: Beam Interactions with Materials and Atoms*, 2–7. doi:10.1016/j.nimb.2015.02.066

Christl, M., Lachner, J., Vockenhuber, C., Goroncy, I., Herrmann, J., & Synal, H. A. (2013). First data of Uranium-236 in the North Sea. *Nuclear Instruments and Methods in Physics Research, Section B: Beam Interactions with Materials and Atoms*, *294*, 530–536. doi:10.1016/j.nimb.2012.07.043

Cochran, K., Hirschberg, D., Livingston, H., Buesseler, K., & Key, R. (1995). Natural and anthropogenic radionuclide distributions in the nansen basin, arctic ocean scavenging rates and circulation timescales. *Deep-Sea Research Part II: Topical Studies in Oceanography*, *42*(6), 1495–1517.

Comiso, J., Parkinson, C., Markus, T., Cavalieri, D., & Gersten, R. (2015, June 03). *Curent state of sea ice cover*. Retrieved from http://neptune.gsfc.nasa.gov/csb/index.php?section=234

Curry, R.G., McCartney, M.S., Joyce, T.M., 1998. Oceanic transport of subpolar climate signals to mid-depth subtropical waters. Nature 391, 575–577.

Eigl, R., Srncik, M., Steier, P., & Wallner, G. (2013). 236U/238U and 240Pu/239Pu isotopic ratios in small (2 L) sea and river water samples. *Journal of Environmental Radioactivity*, *116*, 54–8. doi:10.1016/j.jenvrad.2012.09.013

Fehn, U., Peters, E. ., Tullai-Fitzpatrick, S., Kubik, P. ., Sharma, P., Teng, R. T. ., … Elmore, D. (1992). 129I and 36Cl concentrations in waters of the eastern Clear Lake area, California: Residence times and source ages of hydrothermal fluids. *Geochimica et Cosmochimica Acta*, *56*, 2069–2079. doi:10.1016/0016-7037(92)90330-L

Fuglestvedt, J., Dalsøren, S., Samset, B., Berntsen, T., Myhre, G., Hodnebrog, Ø., … Bergh, T. (2014). Climate Penalty for Shifting Shipping to the Arctic. *Environmental Science & Technology*, *48*(October). doi:dx.doi.org/10.1021/es502379d

Gómez-Guzmán, J. M., Villa, M., Le Moigne, F., López-Gutiérrez, J. M., & García-León, M. (2013). AMS measurements of 129I in seawater around Iceland and the Irminger Sea. *Nuclear Instruments and Methods in Physics Research Section B: Beam Interactions with Materials and Atoms*, *294*, 547–551. doi:10.1016/j.nimb.2012.07.045

Hansen, B., & Osterhus, S. (2000). North Atlantic Nordic Seas Exchanges. *Progress in Oceanography*, *45*(2), 109–208. doi:10.1016/S0079-6611(99)00052-X

Horwitz, E.P., et al, Separation and preconcentration of uranium from acidic media by extraction chromatography, Analytica *Chimica Acta, Vol.266, pp. 25-37*

Hotchkis, M. a. ., Child, D., Fink, D., Jacobsen, G. ., Lee, P. ., Mino, N., Tuniz, C. (2000). Measurement of 236U in environmental media. *Nuclear Instruments and Methods in Physics Research Section B: Beam Interactions with Materials and Atoms*, *172*(1-4), 659–665. doi:10.1016/S0168-583X(00)00146-4

International Arctic Science Committee. (2010). *Arctic climate impact assessment: Ocean processes of climatic importance in the Arctic.* Retrieved from http://www.eoearth.org/view/article/154991/

Jakobsson M, Cherkis NZ, Woodward J, Macnab R, and Coakley B (2000) New grid of Arctic bathymetry aids scientists and mapmakers. EOS, Transactions of American Geophysical Union 81(9): 89--96.

Jakobsson M, Macnab R, Mayer L, et al. (2008) An improved bathymetric portrayal of the Arctic Ocean: Implications for ocean modelling and geological, geophysical and oceanographic analyses. Geophysical Research Letters 35: L07602 (doi:10.1029/2008 GL0335220).

Jones, E. (2001). Circulation in the arctic ocean. *Polar Research*, *20*(2), 139-146. doi: 10.1111/j.1751-8369.2001.tb00049.x

Karcher, M., Smith, J. N., Kauker, F., Gerdes, R., & Smethie, W. M. (2012). Recent changes in Arctic Ocean circulation revealed by iodine-129 observations and modeling. *Journal of Geophysical Research*, *117*(C8), C08007. doi:10.1029/2011JC007513

Kieser, W. E., Zhao, X.-L., Clark, I. D., Cornett, R. J., Litherland, A. E., Klein, M., … Alary, J.-F. (2015). The André E. Lalonde AMS Laboratory – The new accelerator mass spectrometry facility at the University of Ottawa. *Nuclear Instruments and Methods in Physics Research Section B: Beam Interactions with Materials and Atoms*, *361*, 110–114. http://doi.org/10.1016/j.nimb.2015.03.014

Kieser, W., & Litherland, A. (2007). *Protocol for the Analysis of Iodine-129 at the IsoTrace Laboratory* (3.07 ed.). Toronto, Ontario: IsoTrace Laboratory, University of Toronto.

Kilius, L. R., Litherland, a. E., Rucklidge, J. C., & Baba, N. (1992). Accelerator mass-spectrometric measurements of heavy long-lived isotopes. *International Journal of Radiation Applications and Instrumentation. Part A. Applied Radiation and Isotopes*, *43*(1-2), 279–287. doi:10.1016/0883-2889(92)90100-S

Laidre KL, Stirling I, Lowry L, Wiig, Heide-Jørgensen MP, Ferguson S. 2008. Quantifying the sensitivity of arctic marine mammals to climate-induced habitat change. Ecological Applications 18:S97– S125.

Laidre, K. L., Stern, H., Kovacs, K. M., Lowry, L., Moore, S. E., Regehr, E. V, … Ugarte, F. (2015). Arctic marine mammal population status, sea ice habitat loss, and conservation recommendations for the 21st century. *Conservation Biology*, *00*(0), 1–14. doi:10.1111/cobi.12474

Lasserre, F. (2014). Case studies of shipping along Arctic routes. Analysis and profitability perspectives for the container sector. *Transportation Research Part A: Policy and Practice*, *66*(1), 144–161. doi:10.1016/j.tra.2014.05.005

Lavender, K. L., R. E. Davis, and W. B. Owens, 2000: Mid-depth recirculation observed in the interior Labrador and Irminger Seas by direct velocity measurements. Nature, 407, 66–69.

Lazier, J., Hendry, R., Clarke, A., Yashayaev, I., & Rhines, P. (2002). Convection and restratification in the Labrador Sea , 1990 – 2000. *Deep-Sea Research Part I: Oceanographic Research Papers*, *49*, 1819–1835.

McBean, G., G. Alekseev, D. Chen, E. Førland, J. Fyfe, P.Y. Groisman, R. King, H. Melling, R. Vose and P.H. Whitfield, 2005:Arctic climate: past and present. Arctic Climate Impacts Assessment (ACIA), C. Symon, L. Arris and B. Heal, Eds., Cambridge University Press, Cambridge, 21-60.

National Snow and Ice Data Center. (2015). *What is the arctic?*. Retrieved from https://nsidc.org/cryosphere/arctic-meteorology/arctic.html

Osadetz, K., Dixon, J., Dietrich, J., Snowdon, L., Dallimore, S., & Majorowicz, J. Natural Resources Canada, Geological Survey of Canada. (2005). *A review of mackenzie delta-beaufort sea petroleum province conventional and non-conventional (gas hydrate) petroleum reserves and undiscovered resources: A contribution to the resource assessment of the proposed mackenzie delta-beaufort sea marine protected area*. Retrieved from Natural Resources Canada website: http://www.dfo-mpo.gc.ca/Library/281345.pdf

Pickart, R. S., & Spall, M. A. (2007). Impact of Labrador Sea Convection on the North Atlantic Meridional Overturning Circulation. *Journal of Physical Oceanography, 37*(9), 2207–2227. doi:10.1175/JPO3178.1

Pickart, R.S., Torres, D.J., Clarke, R.A., 2002. Hydrography of the Labrador Sea during active convection. Journal of Physical Oceanography 32, 428–457.

Raisbeck, G. M., Yiou, F., Zhou, Z. Q., & Kilius, L. R. (1995). 129I from nuclear fuel reprocessing facilities at Sellafield (U.K.) and La Hague (France); potential as an oceanographie tracer. *Journal of Marine Systems, 6*(5-6), 561–570. doi:10.1016/0924-7963(95)00024-J

Rudels B, Jones EP, Anderson LG, and Kattner G (1994) On the intermediate depth waters of the Arctic Ocean. In: Johannesen OM, Muench RD, and Overland JE (eds.) AGU Geophysical Monographs 85: The Polar Oceans and Their Role in Shaping the Global Environment, pp. 33--46. Washington, DC: American Geophysical Union

Rudels, B. (2009). Arctic ocean circulation. In J. Steele, K. Turekian & S. Thorpe (Eds.), *Encyclopedia of Ocean Science* (2nd ed., pp. 211-225). Academic Press.

Rudels, B. (2015). Arctic ocean circulation, processes and water masses: A description of observations and ideas with focus on the period prior to the international polar year 2007-2009. *Progress in Oceanography, 132,* 22-67.

Rudels, B. Anderson, L. G. & Jones, E. P. 1996: Formation and evolution of the surface mixed layer and halocline of the Arctic Ocean. J. Geophys. Res. 101(C4), 8807–8821.

Rudels, B., Jones, E. P., Schauer, U., & Eriksson, P. (2004). Atlantic sources of the Arctic Ocean surface and halocline waters. *Polar Research, 23*(2), 181–208. doi:10.1111/j.1751-8369.2004.tb00007.x

Sakaguchi, A., Kadokura, A., Steier, P., Takahashi, Y., Shizuma, K., Hoshi, M., Yamamoto, M. (2012). Uranium-236 as a new oceanic tracer: A first depth profile in the Japan Sea and comparison with caesium-137. *Earth and Planetary Science Letters, 333-334*(8), 165–170. doi:10.1016/j.epsl.2012.04.004

Sakaguchi, A., T. Nomura, P. Steier, R. Gloser, K. Sasaki, T. Watanabe, T. Nakakuki, Y. Takahashi, and H. Yamano (2015), Temporal and vertical distributions of anthropogenic 236U in the Japan Sea using a coral core and seawater samples, J. Geophys. Res. Oceans, 120, doi:10.1002/ 2015JC011109

Saundry, P. (2010, March 2). Atlantic meridional overturning circulation (M. Pidwirny, Ed.). Retrieved November 4, 2015, from http://www.eoearth.org/view/article/150290/

Smith, J. N., Ellis, K. M., & Boyd, T. (1999). Circulation features in the central Arctic Ocean revealed by nuclear fuel reprocessing tracers from Scientific Ice Expeditions 1995 and 1996. *Journal of Geophysical Research*, *104*(C12), 29663. doi:10.1029/1999JC900244

Smith, J. N., Ellis, K. M., & Kilius, L. R. (1998). 129I and 137Cs tracer measurements in the Arctic Ocean. *Deep-Sea Research Part I: Oceanographic Research Papers*, *45*(6), 959–984. doi:10.1016/S0967-0637(97)00107-6

Smith, J. N., Jones, E. P., Moran, S. B., Smethie Jr., W. M., & Kieser, W. E. (2005). Iodine 129/CFC 11 transit times for Denmark Strait Overflow Water in the Labrador and Irminger Seas. *Journal of Geophysical Research*, *110*(C5), C05006. doi:10.1029/2004JC002516

Smith, J. N., McLaughlin, F. a., Smethie, W. M., Moran, S. B., & Lepore, K. (2011). Iodine-129, 137Cs, and CFC-11 tracer transit time distributions in the Arctic Ocean. *Journal of Geophysical Research: Oceans*, *116*(4), 1–19. doi:10.1029/2010JC006471

Steier, P., Bichler, M., Fifield, L. K., Golser, R., Kutschera, W., Priller, A., Maria, E. (2008). U in environmental samples, *266*, 2246–2250. doi:10.1016/j.nimb.2008.03.002

Tomszak, M., & Godfrey, S. (1994). Arctic Oceanography. In *Regional oceanography: An introduction* (pp. 100-104). Oxford; Elsevier.

Weeks, W. (2010). *On sea ice*. Fairbanks, AK: University of Alaska Press.

Yashayaev, I. (2007). Progress in Oceanography Hydrographic changes in the Labrador Sea , 1960 – 2005, *73*, 242–276. doi:10.1016/j.pocean.2007.04.015

Yashayaev, I., Head, E.J.H., Azetsu-Scott, K., Ringuette, M., Wang, Z., Anning, J., and Punshon, S. 2014. Environmental Conditions in the Labrador Sea during 2013. DFO Can. Sci. Advis. Sec. Res. Doc. 2014/105. v +35 p.

Yashayaev, I., Seidov, D., & Demirov, E. (2015). Progress in Oceanography A new collective view of oceanography of the Arctic and North Atlantic basins. *Progress in Oceanography*, *132*, 1–21. doi:10.1016/j.pocean.2014.12.012

Yashayev, I., Holliday, P., Bersch, M., and van Aken,. H. (2008). The History of the Labrador Sea Water: Production, Spreading, Transformation and Loss. In R. Dickson, J. Meincke, and P. Rhines (Eds.), *Arctic-Subarctic Ocean Fluxes* (pp. 569-612). Dordrecht, The Netherlands: Springer

Zavodska L, Kosorinova E, Scerbakova L, Lesny J (2008) Environmental chemistry of uranium. HV ISSN 1418-7108: HEJ Manuscript No: ENV-081221-A

Zhao, X., Kilius, L., Litherland, A., & Beasley, T. (1997). AMS measurement of environmental U-236 Preliminary results and perspectives. *Nuclear Instruments and …*. Retrieved from http://www.sciencedirect.com/science/article/pii/S0168583X96010348

6. Appendix

6.1 Appendix A – Sample Data

Labrador Sea – Uranium

Sample Site	Sample ID	N Latitude	W Longitude	Depth (m)	Sample Mass (kg)	233U added (pg)	HNO3 added (mL)	FeCl3 added (mg Fe)	Bubbling Time	NH4OH added (mL)
L3-05	U1	N 54' 29.5"	W 54' 45.3"	4	14.8	5.22	20	400	20m 19s	25
L3-05	U2	N 54' 29.5"	W 54' 45.3"	4	14.7	5.22	20	400	20m 19s	25
L3-07	U1	N 54' 57.3"	W 54' 17.7"	4	15.2	5.22	20	400	20m 34s	25
L3-07	U2	N 54' 57.3"	W 54' 17.7"	4	15.2	5.22	20	400	20m 34s	25
L3-09	U1	N 55' 15.8"	W 53' 59"	4	15	5.22	20	400	20m 30s	25
L3-09	U2	N 55' 15.8"	W 53' 59"	4	15	5.22	20	400	20m 30s	25
L3-11	U1	N 55' 36.7"	W 53' 37.9"	4	15.4	5.22	20	400	20m 41s	25
L3-11	U2	N 55' 36.7"	W 53' 37.9"	4	15.1	5.22	20	400	20m 41s	25
L3-13	U1	N 56' 6.8"	W 53' 7"	4	15	5.22	20	400	20m 30s	25
L3-13	U2	N 56' 6.8"	W 53' 7"	4	15.3	5.22	20	400	20m 30s	25
L3-15	U1	N 56' 57.4"	W 52' 14.2"	4	15.2	5.22	20	400	21m 30s	25
L3-15	U2	N 56' 57.4"	W 52' 14.2"	4	15	5.22	20	400	22m 00s	25
L3-17	U1	N 57' 48"	W 51' 20.4"	4	14.7	5.22	20	400	21m 33s	25
L3-17	U2	N 57' 48"	W 51' 20.4"	4	16.1	5.22	20	400	21m 33s	25
L3-19	U1	N 58' 38.4"	W 50' 25"	4	15.5	5.22	20	400	21m 50s	25
L3-19	U2	N 58' 38.4"	W 50' 25"	4	15.8	5.22	20	400	21m 50s	25
L3-21	U1	N 59' 29"	W 49' 28.5"	4	15	5.22	20	400	21m 27s	25
L3-21	U2	N 59' 29"	W 49' 28.5"	4	14.9	5.22	20	400	21m 27s	25
L3-24	U1	N 60' 10.5"	W 48' 40.5"	4	15	5.22	20	400	21m 32s	25
L3-24	U2	N 60' 10.5"	W 48' 40.5"	4	15.3	5.22	20	400	21m 32s	25
L3-25	U1	N 60' 17.5"	W 48' 32.5"	4	15.3	5.22	20	400	22m 50s	25
L3-25	U2	N 60' 17.5"	W 48' 32.5"	4	15.2	5.22	20	400	22m 50s	25
L3-26	U1	N 60' 22"	W 48' 27.2"	4	14.9	5.22	20	400	20m 50s	25
L3-26	U2	N 60' 22"	W 48' 27.2"	4	15.1	5.22	20	400	20m 50s	25
L3-27	U1	N 60' 26.8"	W 48' 21.7"	4	15.3	5.22	20	400	20m 40s	25
L3-27	U2	N 60' 26.8"	W 48' 21.7"	4	14.9	5.22	20	400	20m 40s	25

L3-28	U1	N 60' 34"	W 48' 13.7"	4	15.1	5.22	20	400	25m 00s	25
L3-28	U2	N 60' 34"	W 48' 13.7"	4	15.5	5.22	20	400	25m 00s	25

Labrador Sea - Cesium

Sample Site	Sample ID	N Latitude	W Longitude	Depth (m)	Mass of Water (kg)	Cs-133 added (mL)	133Cs added (ug)	HNO3 added (mL)	AMP added (g)
L3-05	Cs 1	N 54' 29.5"	W 54' 45.3"	4	15.1	4.99	99.8	20	4.01
L3-05	Cs 2	N 54' 29.5"	W 54' 45.3"	4	15.1	4.98	99.6	20	4.01
L3-07	Cs 1	N 54' 57.3"	W 54' 17.7"	4	15	4.99	99.8	20	4
L3-07	Cs 2	N 54' 57.3"	W 54' 17.7"	4	15.3	5	100	20	4
L3-09	Cs 1	N 55' 15.8"	W 53' 59"	4	15.2	4.98	99.6	20	4.01
L3-09	Cs 2	N 55' 15.8"	W 53' 59"	4	15.6	5.01	100.2	20	3.98
L3-11	Cs 1	N 55' 36.7"	W 53' 37.9"	4	15.5	5	100	20	4.02
L3-11	Cs 2	N 55' 36.7"	W 53' 37.9"	4	15.4	5	100	20	4.01
L3-13	Cs 1	N 56' 6.8"	W 53' 7"	4	15	4.98	99.6	20	4.02
L3-13	Cs 2	N 56' 6.8"	W 53' 7"	4	15	4.97	99.4	20	4.02
L3-15	Cs 1	N 56' 57.4"	W 52' 14.2"	4	15.4	5	100	20	4
L3-15	Cs 2	N 56' 57.4"	W 52' 14.2"	4	15.4	5	100	20	4
L3-17	Cs 1	N 57' 48"	W 51' 20.4"	4	15.5	5	100	20	4.01
L3-17	Cs 2	N 57' 48"	W 51' 20.4"	4	15.6	5	100	20	4
L3-19	Cs 1	N 58' 38.4"	W 50' 25"	4	14.7	5	100	20	4
L3-19	Cs 2	N 58' 38.4"	W 50' 25"	4	15.4	5	100	20	4.01
L3-21	Cs 1	N 59' 29"	W 49' 28.5"	4	15.1	5	100	20	4
L3-21	Cs 2	N 59' 29"	W 49' 28.5"	4	14.9	5	100	20	4
L3-24	Cs 1	N 60' 10.5"	W 48' 40.5"	4	15.1	4.98	99.6	20	4.01
L3-24	Cs 2	N 60' 10.5"	W 48' 40.5"	4	15.1	4.93	98.6	20	4.01
L3-26	Cs 1	N 60' 22"	W 48' 27.2"	4	15.2	5.96	119.2	20	4.02
L3-26	Cs 2	N 60' 22"	W 48' 27.2"	4	14.8	4.98	99.6	20	4.01
L3-27	Cs 1	N 60' 26.8"	W 48' 21.7"	4	15.1	5	100	20	4
L3-27	Cs 2	N 60' 26.8"	W 48' 21.7"	4	15.1	5	100	20	3.97

Beaufort Sea - Cesium

Sample ID	Station ID	Depth (m)	Sample Mass (kg)	133Cs added (ng)	HNO3 added (ml)	AMP added (g)
Cs 242	STA-A	5	15.9	100	20	4.01
Cs 237	STA-A	64	15	100	20	4.02
Cs 234	STA-A	185	15.9	100	20	4.01
Cs 232	STA-A	200	14.8	100	20	4.01
Cs 228	STA-A	400	14.9	100	20	4.01
Cs 225	STA-A	600	15.5	100	20	4
Cs 223	STA-A	800	17.4	100	20	4.01
Cs 221	STA-A	1000	14.5	100	20	4.01

Beaufort Sea - Uranium

Sample ID	Station ID	Depth (m)	Sample Mass (kg)	233U added (pg)	TiCl3 added (ml)	HNO3 added (ml)	FeCl3 added (ml)	Bubbling Time	NH4OH added (ml)
U 221	STA-A	1000	14.1	5.22	0.6	20	400	24m 30s	35
U 223	STA-A	800	17.1	5.22	0.6	20	400	25m 48s	35
U 225	STA-A	600	15.1	5.22	0.6	20	400	26m 17s	35
U 228	STA-A	400	14.5	5.22	0.6	20	400	24m 0s	35
U 232	STA-A	200	14.4	5.22	0.6	20	400	24m 0s	35
U234	STA-A	185	15.5	5.22	0.6	20	400	25m 0s	35
U237	STA-A	64	14.6	5.22	0.6	20	400	27m 0s	35
U 242	STA-A	5	15.5	5.22	0.6	20	400	23m 30s	35

6.2 Appendix B – Experimental Data

^{129}I

Labrador Sea

Sample ID	Depth (m)	Sample Mass (g)	Corrected 129I (atm/L)	Uncertainty (atm/L)
L3-05	4	199.43	9.67E+08	3.39E+04
L3-07	4	203.21	9.50E+08	3.36E+04
L3-09	4	205.00	7.39E+08	3.00E+04
L3-11	4	201.78	4.14E+08	2.32E+04
L3-13	4	209.83	3.38E+08	2.12E+04
L3-15	4	200.79	3.52E+08	2.16E+04
L3-17	4	201.13	3.82E+08	2.24E+04
L3-19	4	199.26	7.12E+08	2.95E+04
L3-21	4	199.98	7.84E+08	3.08E+04
L3-24	4	201.66	1.59E+09	4.27E+04
L3-25	4	201.36	1.86E+09	4.59E+04
L3-26	4	200.06	2.33E+09	5.10E+04
L3-27	4	200.55	2.21E+09	4.97E+04
L3-28	4	201.72	2.11E+09	4.87E+04
L3-17-510m	510	202.30	3.18E+08	2.07E+04
L3-17-870m	870	203.38	3.20E+08	2.07E+04
L3-17-1300m	1300	200.99	3.20E+08	2.07E+04
L3-17-1550m	1550	203.40	3.04E+08	2.03E+04
L3-17-2040m	2040	200.76	2.05E+08	1.72E+04
L3-17-2520m	2520	205.58	2.59E+08	1.90E+04
L3-17-2940m	2940	204.05	3.37E+08	2.12E+04
L3-17-3120m	3120	203.83	3.96E+08	2.27E+04
L3-17-3380m	3380	203.72	6.59E+08	2.85E+04
L3-17-3490m	3490	214.54	8.78E+08	3.24E+04
L3-17-3590m	3590	203.47	1.04E+09	3.51E+04

L3-17-3670m	3670	201.81	1.04E+09	3.51E+04
L3-24-310m	310	201.50	3.92E+08	2.27E+04
L3-24-560m	560	203.75	3.70E+08	2.21E+04
L3-24-880m	880	200.90	3.43E+08	2.14E+04
L3-24-1060m	1060	202.14	3.10E+08	2.05E+04
L3-24-1460m	1460	200.79	2.64E+08	1.91E+04
L3-24-1860m	1860	200.16	4.23E+08	2.34E+04
L3-24-2240m	2240	205.10	4.55E+08	2.42E+04
L3-24-2400m	2400	200.30	4.93E+08	2.50E+04
L3-24-2540m	2540	201.68	5.69E+08	2.67E+04
L3-24-2760m	2760	201.79	5.15E+08	2.55E+04
L3-24-2840m	2840	199.82	5.47E+08	2.62E+04
L3-24-2900m	2900	202.78	6.22E+08	2.78E+04
17-24m (2012)	24		5.03E+08	
17-870m (2012)	870		2.43E+08	
17-2290m (2012)	2290		1.34E+08	
17-3120m (2012)	3120		2.69E+08	
17-3490m (2012)	3490		6.71E+08	
17-3590m (2012)	3590		8.00E+08	
17-3670m (2012	3670		8.39E+08	

^{137}Cs

Beaufort Samples (Cs ###) Decay corrected from 2014/09/08, Labrador Sea (L3-##) Samples Decay corrected from between 2014/05/09 and 2014/05/15, Cs 1 and Cs 2 refer to duplicates from the same station

			ORTEC Counter		
Sample ID	Station	Depth	Bq/m3	Decay Corrected Bq/m3	Uncertainty Bq/m3
Cs 221	STA-A	1013	2.15	2.21	0.20
Cs 223	STA-A	805.919	2.25	2.31	0.26
Cs 225B	STA-A	608.748	2.18	2.24	0.20
Cs 228	STA-A	403.992	2.44	2.50	0.27
Cs 232	STA-A	202.285	1.52	1.56	0.16
Cs 234	STA-A	187.213	0.99	1.02	0.15
Cs 237	STA-A	65.397	1.08	1.11	0.23
Cs 242	STA-A	6.414	1.07	1.10	0.16
L3-05-Cs1	L3-05	5	1.11	1.15	0.17
L3-05-Cs2	L3-05	5	0.90	0.93	0.14
L3-07-Cs1	L3-07	5	0.97	1.01	0.16
L3-07-Cs2	L3-07	5	1.26	1.31	0.17
L3-09-Cs1	L3-09	5	0.97	1.00	0.12
L3-09-Cs2	L3-09	5	0.92	0.95	0.18
L3-11-Cs1	L3-11	5	0.92	0.96	0.17
L3-11-Cs2	L3-11	5	1.05	1.09	0.15
L3-13-Cs1	L3-13	5	0.88	0.91	0.17
L3-13-Cs2	L3-13	5	0.77	0.79	0.18
L3-15-Cs1	L3-15	5	0.87	0.90	0.15
L3-15-Cs2	L3-15	5	1.07	1.11	0.18
L3-17-Cs1	L3-17	5	0.82	0.85	0.17
L3-17-Cs2	L3-17	5	0.79	0.82	0.14
L3-19-Cs1	L3-19	5	1.00	1.04	0.19
L3-19-Cs2	L3-19	5	0.74	0.76	0.18

L3-21-Cs1	L3-21	5	0.83	0.86	0.18
L3-21-Cs2	L3-21	5	0.67	0.69	0.17
L3-24-Cs1	L3-24	5	0.90	0.93	0.20
L3-24-Cs2	L3-24	5	1.12	1.16	0.15
L3-26-Cs1	L3-26	5	0.94	0.98	0.17
L3-26-Cs2	L3-26	5	0.99	1.03	0.18
L3-27-Cs1	L3-27	5	0.99	1.03	0.31
L3-27-Cs2	L3-27	5	0.98	1.02	0.16

CANBERA Counter

Sample ID	Station	Depth	Bq/m3	Decay Corrected Bq/m3	Uncertainty Bq/m3
Cs 221	STA-A	1013	1.97	2.02	0.21
Cs 223	STA-A	805.919	2.11	2.17	0.20
Cs 225B	STA-A	608.748	2.28	2.35	0.21
Cs 228	STA-A	403.992	2.53	2.60	0.18
Cs 232	STA-A	202.285	1.56	1.60	0.18
Cs 234	STA-A	187.213	1.11	1.14	0.11
Cs 237	STA-A	65.397	0.95	0.98	0.14
Cs 242	STA-A	6.414	0.83	0.85	0.10

Cs Yield Tracer

Sample ID	133Cs (ppb)	133Cs in Sample (ug/L)	Expected 133Cs in sample (ug/L)	Measured 133Cs/Expected 133Cs
L3-05-Cs1	34.879	3.415	4.6565	0.733
L3-05-Cs2	0.017	0.001	0.0913	0.015
L3-07-Cs1	16.594	2.927	4.2137	0.695
L3-07-Cs2	18.610	3.307	4.2108	0.785
L3-09-Cs1	22.680	4.385	4.6717	0.939
L3-09-Cs2	21.809	4.446	4.8334	0.920

L3-11-Cs1	20.283	3.906	4.4685	0.874
L3-11-Cs2	20.511	3.711	4.2943	0.864
L3-13-Cs1	22.547	3.853	4.0348	0.955
L3-13-Cs2	21.786	3.827	4.1812	0.915
L3-15-Cs1	18.870	3.734	4.6744	0.799
L3-15-Cs2	21.850	4.031	4.3893	0.918
L3-17-Cs1	18.111	3.562	4.5498	0.783
L3-17-Cs2	17.118	3.095	4.3331	0.714
L3-19-Cs1	17.942	3.445	4.5154	0.763
L3-19-Cs2	17.990	3.271	4.3260	0.756
L3-21-Cs1	16.320	3.420	4.9127	0.696
L3-21-Cs2	15.926	2.416	3.5872	0.674
L3-24-Cs1	23.087	4.435	4.6202	0.960
L3-24-Cs2	21.667	4.179	4.5573	0.917
L3-26-Cs1	18.634	3.397	4.2706	0.795
L3-26-Cs2	20.170	3.522	4.1223	0.854
L3-27-Cs1	20.999	3.484	3.9435	0.883
L3-27-Cs2	21.456	3.570	4.0081	0.891
Cs 221	1.060	0.174	0.0039	44.689
Cs 223	1.402	0.170	0.0029	59.376
Cs 225	1.416	0.157	0.0026	59.364
Cs 228	1.308	0.167	0.0030	55.780
Cs 232	1.308	0.159	0.0029	55.008
Cs 234	1.382	0.141	0.0024	59.676
Cs 237	1.274	0.143	0.0027	53.067
Cs 242	1.219	0.132	0.0026	51.085
Cs 438	1.311	0.154	0.0027	56.995
Cs 441	1.482	0.167	0.0027	62.296
Cs 471	1.726	0.162	0.0022	72.472
Cs 474	1.538	0.148	0.0023	64.632

^{236}U

Run 1 ^{236}U Results

Sample ID	Counts	Time (sec)	atm/L	error (atm/L)	Atom Ratio (236/238)	238 ppb	129I (atm/L)	129I/236U
07-U2	539	2038.89	2.25E+06	2.86E+05	3.08E-10	2.873164	9.50E+08	421.43
09-U2	3043	2038.89	5.07E+06	4.27E+05	6.54E-10	3.04E+00	7.39E+08	145.86
13-U1	586	2038.89	7.87E+05	1.78E+05	1.43E-10	2.16E+00	3.38E+08	430.28
15-U2	703	2038.89	1.24E+06	2.00E+05	1.69E-10	2.87E+00	3.52E+08	284.91
17-U2	1954	2038.89	8.55E+06	6.01E+05	1.20E-09	2.80E+00	3.82E+08	44.65
19-U2	965	2038.89	4.48E+06	3.85E+05	5.99E-10	2.94E+00	7.12E+08	158.76
24-U2	2484	2038.89	8.33E+06	8.28E+05	1.64E-09	1.99E+00	1.59E+09	191.32
25-U2	741	1961.22	1.53E+06	3.37E+05	4.67E-10	1.29E+00	1.86E+09	1215.78
26-U2	504	2038.89	4.01E+06	5.17E+05	5.75E-10	2.74E+00	2.33E+09	580.99
27-U2	718	2038.89	3.33E+06	5.98E+05	4.80E-10	2.72E+00	2.21E+09	662.54
28-U1	739	2038.89	1.96E+06	3.27E+05	2.70E-10	3.00E+00	2.00E+09	1076.83

Run 2 ^{236}U Results

Sample ID	Counts	Time (sec)	atm/L	error atm/L	Atom Ratio (236/238)	238 ppb	129I atm/L	129I/ Run 3 236U
07-U2	1	1165.08	1.05E+06	2.68E+06	1.43E-10	2.87316353	9.50E+08	905.64
09-U2	10	1165.08	4.68E+06	2.95E+06	6.04E-10	3.03734625	7.39E+08	157.97
13-U1	5	1165.08	9.27E+05	1.37E+06	1.68E-10	2.16384444	3.38E+08	365.22
17-U2	11	1165.08	6.37E+06	3.86E+06	8.93E-10	2.7976217	3.82E+08	59.94
24-U2	22	1165.08	5.61E+06	2.45E+06	1.71E-09	1.28709521	1.59E+09	284.22
27-U2	6	1165.08	2.83E+06	3.88E+06	4.09E-10	2.71881175	2.21E+09	779.03
28-U1	2	1165.08	3.02E+06	6.31E+06	4.16E-10	2.84360278	2.11E+09	699.27

6.3 Appendix C – Relevant Materials

Materials:

^{137}Cs Standard (Amersham CDZ24)

^{233}U Standard (Eckert & Ziegler, item no, 7233)

^{133}Cs Standard (PlasmaCAL, item no. 140-051-551)]

^{127}I Standard (UOttawa, ISO-6II-1)

$FeCl_3$ (Sigma-Aldrich, item no. 236489)

AMP (GFS Chemicals, item no. A0438)

HNO_3 (Fisher Scientific, item no. 351288-212)

NH_4OH (Fisher Scientific, item no. A669-212)

6.4 Appendix D – Step by step Field Methodology

^{137}Cs

18L bucket
Place garbage back into bucket, tape sides
Fill with 15L of sea water
Add tracer stable Cs - preweighed
Subsample 20 mL into LSC vial for U and Cs etc
add conc. HNO3 (20ml)
Mix water and acid
test pH (want less than 2)
Add AMP (4 grams)
Mix
Cover with Lid
Let settle
Syphon of the clear surface water
wash sides of the plastic bag
Transfer to 2 litre graduated cylindar
Let settle
Syphon of the clear surface water
transfer to 250 ml bottle or 1 litre bottles
Transfer to 50ml centrifuge tubes for storage
Rinse the bucket with seawater and dry it out.

^{236}U

18L bucket
Place garbage back into bucket, tape sides
Fill with 15L of sea water
add 0.2g of U233 tracer
Subsample 20ml into LSC vial
add conc. HNO3 (20ml)
Mix water and acid
test pH (want less than 2)
add 10ml of FeCl3 (400mg Fe)
bubble N2 through water for 20 minutes
add 25ml 38% NH3OH to raise pH
mix lightly
test pH (want 8-9)
Cover with lid
let rusty coloured precipitate form and settle
syphon off clear surface water
wash sides of bag
transfer to 2L graduated cylinder
let settle
continue to syphon off water until precipitate can fit in 2-3 50ml centrifuge tubes